Natural Hazards (2006) 37: 277–314
DOI 10.1007/s11069-005-4646-z

Probabilistic Analysis of Tsunami Hazards*

ERIC L. GEIST★ and TOM PARSONS
U.S. Geological Survey, 345 Middlefield Rd., MS 999Menlo Park, CA, 94025, USA

(Received: 31 August 2004; accepted: 14 March 2005)

Abstract. Determining the likelihood of a disaster is a key component of any comprehensive hazard assessment. This is particularly true for tsunamis, even though most tsunami hazard assessments have in the past relied on scenario or deterministic type models. We discuss probabilistic tsunami hazard analysis (PTHA) from the standpoint of integrating computational methods with empirical analysis of past tsunami runup. PTHA is derived from probabilistic seismic hazard analysis (PSHA), with the main difference being that PTHA must account for far-field sources. The computational methods rely on numerical tsunami propagation models rather than empirical attenuation relationships as in PSHA in determining ground motions. Because a number of source parameters affect local tsunami runup height, PTHA can become complex and computationally intensive. Empirical analysis can function in one of two ways, depending on the length and completeness of the tsunami catalog. For site-specific studies where there is sufficient tsunami runup data available, hazard curves can primarily be derived from empirical analysis, with computational methods used to highlight deficiencies in the tsunami catalog. For region-wide analyses and sites where there are little to no tsunami data, a computationally based method such as Monte Carlo simulation is the primary method to establish tsunami hazards. Two case studies that describe how computational and empirical methods can be integrated are presented for Acapulco, Mexico (site-specific) and the U.S. Pacific Northwest coastline (region-wide analysis).

Key words: tsunami, probabilistic hazard analysis, seismic hazard analysis, Monte Carlo, tide gauge, empirical, power-law

1. Introduction

Both deterministic and probabilistic analysis have been used in the past to assess the hazards posed by tsunamis, depending on the objective. For example, tsunami evacuation maps have recently been derived from tsunami inundation maps based on the maximum credible tsunami for a given region (i.e., deterministic scenarios). Insurance applications, in contrast, typically focus on the 1% annual probability of exceedance or the 100-year base flood standard (U.S. Interagency Advisory Committee on Water Data, 1982). Other land-use planning objectives may consider other probabilistic standards such as the 10-year or 500-year floods (10, 0.2% annual

★ Author for correspondence: E-mail: egeist@usgs.gov

probability, respectively). Though there appears to be a distinct difference in these approaches, some intuitive measure of probability is involved in the former case in terms of assigning a maximum credible tsunami for evacuation maps. For example, asteroid tsunamis which may have significant probabilities in a 1000-year time frame (Ward and Asphaug, 2000) are usually not considered for maximum inundation maps, whereas other sources such as large earthquakes which have significant 100-year probabilities usually are included. Other sources, such as submarine landslides and volcanogenic processes, are much more difficult to assign average repeat times and probabilities (Ward, 2001), primarily because of a lack of age dates for these sources in specific regions. In addition to unstated likelihoods associated with deterministic analyses, another problem in assigning a maximum credible event is compounded conservatism (Bogen, 1994). In cases where deterministic scenarios are not based on historic events, there may be a tendency to use upper-bound limits on each of the input source parameters (in the case of landslides, for example, slide velocity, cohesiveness of slide block, slide volume, friction, etc.). Under compounded conservatism, the source probability for the entire scenario is considerably smaller than the probability for each of the input variates used in the analysis. Probabilistic analysis of tsunamis is therefore not only important in determining an annualized risk as with insurance applications, but it is also important in explicitly defining the probability associated with individual scenarios.

Whereas probabilistic analysis of tsunami hazards yields information on likelihood in addition to the other components of hazard assessment (e.g., location, extent, severity) (Kockelman, 1989), the results of probabilistic analysis may be difficult to interpret. Typically, probabilistic hazard curves at a particular site or hazard exeedance maps for a given probability are computed using many different sources. The difficulty in interpreting the results is that the hazard does not represent a single event that is easily understandable in terms of its evolution from generation to runup and inundation. Tinti and Armigliato (2003) assert that detailed, deterministic modeling based on a particular source scenario best serves the purposes of coastal engineers to develop effective tsunami counter-measures. It is likely that for multiple mitigation objectives, both deterministic and probabilistic analyses are needed. In a multi-objective hazard analysis, deaggregation of probabilistic results (cf., Harmsen and Frankel, 2001) is an effective tool for developing scenarios for deterministic modeling.

In contrast to other natural hazards where probabilistic analysis has been applied, particularly earthquake hazards, there are several issues unique to tsunami hazard analysis. First, the area affected by tsunami hazards need not be near the source (i.e., at distances several times the source dimension). This is the case for coastal margins that are affected by dis-

tant, transoceanic tsunamis. The methods used to analyze the hazards from these far-field source and the associated uncertainties are necessarily different than the methods and uncertainties for tsunamis generated by local sources. These differences are best described for the most common tsunami generating mechanism: earthquakes. In comparison to local tsunamis, far-field tsunamis have a simpler parameterization according to the earthquake's mechanism, scalar seismic moment, and radiation pattern (Ben-Menahem and Rosenman, 1972, Comer, 1980; Ward, 1980, 1982; Pelayo and Wiens, 1992; Abe, 1995; Polet and Kanamori, 2000). Other than the general cumulative frequency–magnitude relationship for earthquakes known as the Gutenberg–Richter relationship (Rundle, 1989; Kagan, 1999), assigning specific probabilities to circum-Pacific, subduction-zone earthquakes has proven to be a difficult topic (Kagan and Jackson, 1995; Schwartz, 1999; Rong *et al*., 2003). In contrast, for local tsunamis where offshore faults may have established historic and paleoseismologic recurrence rates, the larger problem is constraining the many other seismic parameters that affect local tsunami generation (Kajiura, 1981; Geist, 1999; Geist and Bilek, 2001; Geist, 2002).

A second problem in establishing tsunami probabilities is the limited amplitude range of tsunami measurements. The two primary methods for recording tsunami wave heights are from tide gauge stations and from post-event surveys that measure the elevation of high-water line marks, broken tree branches, etc. It is important to recognize that these are two different types of measurements. Whereas tide-gauge stations measure tsunami waveform amplitudes from a stilling well in the water, the post-event surveys are onshore measurements of wave elevations or flow depths during runup. In some cases, such as vegetation removal or intrusion by salt water, maximum runup can be recorded. Errors associated with this type of measurement are discussed by Baptista *et al*. (1993) and Borrero (2001) and are usually in the 1-m range. For tide gauge data, minimum tsunami amplitudes reported in catalogs are approximately 0.1 m (Burroughs and Tebbens, 2005), owing primarily to ambient wave activity in harbors. With maximum tsunami amplitudes in the 30–40 m range, conventional measurements span less than three orders of magnitude in amplitude. New bottom pressure sensors that record tsunamis in the open ocean and away from wind-generated wave influence will undoubtedly increase this amplitude range (Hino *et al*., 2001; Hirata *et al*., 2003). The existing range represented in tsunami catalogs, however, is much less than, for example, earthquakes that span many orders of magnitude (Abercrombie, 1995).

The two aforementioned issues are directly linked to two components of PTHA: computationally based methods and empirical analysis of tsunami runup and amplitude data. PTHA is derived from probabilistic seismic hazard analysis (PSHA) as discussed by a number of authors (Lin and

Tung, 1982; Rikitake and Aida, 1988; Ward and Asphaug, 2000; Downes and Stirling, 2001; Ward, 2002; Geist, 2005). Computationally based methods rely on knowledge of source parameters, recurrence rates and their uncertainties. Empirical analysis is based solely on the historical record of tsunamis at a particular location. Hence, it is critically dependent on the available range of measurements as well as catalog completeness.

The objective of this paper is to demonstrate how computational methods and empirical analysis can be used jointly to yield a comprehensive hazard assessment. Both of these approaches have advantages. For example, computational methods are valuable where there are few historical records or for including many possible sources with a wide range of likelihood of occurring. In contrast to deterministic scenarios, computational probabilistic methods also have the advantage that they can include parameter sensitivity estimates. The advantage of empirical analysis is that no *a priori* knowledge of source type or location is needed to calculate probabilities. We first discuss PTHA and review past empirical analysis techniques for tsunami data. We then develop two contrasting case studies where both computational and empirical methods are used. The first is a site-specific study for Acapulco where there is a long record of tsunamis. The second case study is a regional assessment for the U.S. Pacific Northwest coastline where there is sparse tsunami data.

2. Probabilistic Tsunami Hazard Analysis (PTHA)

The computational method in PTHA generally follows the PSHA method originally developed by Cornell (1968). PSHA is a widely used method for assessing seismic hazards and has been comprehensively described and reviewed in several reports (National Research Council (NRC), 1988, 1997; Senior Seismic Hazard Analysis Committee (SSHAC), 1997). In rudimentary terms, the method consists of three steps: (1) specification of the earthquake source parameters and associated uncertainties; (2) specification of the attenuation relationships; and (3) the probabilistic calculations (see http://www.relm.org/tutorial_materials/). Step 2 of PSHA often involves empirical analysis of existing data to determine ground motion (e.g., Boore *et al*., 1997). Various aspects of PSHA have been discussed by a number of authors, including the distinction between aleatory and epistemic uncertainty (Toro *et al*., 1997; Anderson and Brune, 1999; Anderson *et al*., 2000), use of synthetic earthquake catalogs (Ward, 1991, 1996, 2000), Monte Carlo methods (Savage, 1991, 1992; Cramer *et al*., 1996; Ebel and Kafka, 1999), and logic trees (Coppersmith and Youngs, 1986), application to fault rupture hazards (Youngs *et al*., 2003), and deaggregation of probabilistic results (Harmsen and Frankel, 2001).

2.1. THEORY

Computational methods similar to PSHA have been used to develop PTHA (Lin and Tung, 1982; Rikitake and Aida, 1988; Ward and Asphaug, 2000; Downes and Stirling, 2001; Ward, 2001, 2002; Geist, 2005). The approach discussed by Ward (2001, 2002), is perhaps the most straightforward and is summarized as follows. The first step (tsunami generation) is to determine the maximum tsunami amplitude ($h_{\max}(\mathbf{r}_0,\psi_s)$) at a particular source location given by location vector $\mathbf{r}_0$ and a parameter space ψ_s (Ward, 2001). For earthquake sources, $h_{\max}(\mathbf{r}_0,\psi_s)$ is equal to the coseismic vertical displacement field for offshore regions ($h_{\max}(\mathbf{r}_0, \psi_s) = 0$ for onshore regions). If the spatial wavelength of vertical displacement is less than approximately three times the water depth, then a tsunami generation Green's function has to be applied to compute $h_{\max}(\mathbf{r}_0, \psi_s)$ from the vertical displacement field (Kajiura, 1963; Satake, 2002). Also, in regions of steep bathymetry over the source area, Tanioka and Satake (1996) show that coseismic horizontal displacement has to be included in the computation of $h_{\max}(\mathbf{r}_0, \psi_s)$. Because the phase velocity of tsunami waves is much less than earthquake rupture velocities, finite rupture duration has a minimal effect on $h_{\max}(\mathbf{r}_0, \psi_s)$ (Geist, 1999). During the propagation step, tsunami amplitude is modified by attenuation and shoaling factors. In addition, nearshore tsunami amplitudes are significantly affected by small-scale changes in bathymetry resulting in local amplification, as well as resonance in bays, inlets, and harbors (Rabinovich, 1997). This is analogous to site effects in PSHA.

From a numerical propagation model, a set of source parameters (ψ_s^{crit}) is determined such that at a particular coastal location (given by location vector $\mathbf{r}$), $h_{\max}(\mathbf{r}, \psi_s^{\text{crit}}) \geq h_{\text{crit}}$. This highlights a key difference between PTHA and PSHA. For tsunami computations, displacement of the water column is first computed at the source and then propagated using numerical simulations to coastal sites, whereas for PSHA, peak ground acceleration at a particular site is typically established using empirical attenuation relations that are based only on the magnitude of the source and distance between the source and site (i.e., $r = ||\mathbf{r}-\mathbf{r}_0||$). The rate at which a particular source occurs $\dot{n}(\mathbf{r}_0, \psi_s)$, usually follows a power-law function such as the Gutenberg–Richter (G–R) relation for earthquake magnitude. The total rate at a particular source location that results in wave heights that exceed h_{crit} at our coastal location is calculated by integrating over the parameter space

$$\dot{N}(\mathbf{r}, \mathbf{r}_0, h_{\text{crit}}) = \int_{\psi_s^{\text{crit}}}^{\psi_s^{\max}} \dot{n}(\mathbf{r}_0, \psi_s) \mathrm{d}\psi_s. \tag{1}$$

Then, $\dot{N}(\mathbf{r}, h_{\text{crit}}) = \int \dot{N}(\mathbf{r}_0, h_{\text{crit}}) d\mathbf{r}_0$ represents the rate or number of tsunamis per year at which wave heights are exceeded at a coastal location determined by integrating Equation (1) over all source locations of interest. If we assume a Poissonian arrival time process, the probability that a tsunami with amplitude h_{crit} or greater occurring in time period T is given by the exponential function:

$$P(\mathbf{r}, T, h_{\text{crit}}) = 1 - e^{-\dot{N}(\mathbf{r}, h_{\text{crit}})T}. \tag{2}$$

For far-field seismogenic tsunamis, the parameter space can be simply defined as the moment magnitude of the earthquake magnitude ($\psi_s = M_w$) and the source recurrence rate is given by the G–R distribution $\dot{n}(M_w) = 10^{a+bM_w}$ (Ward, 2002). For asteroid-impact tsunamis, $\dot{n}(\mathbf{r}_0, \psi_s)$ is the annual impact rate per square meter of ocean for bodies of variable radii (Ward and Asphaug, 2000). For landslide tsunamis (Ward, 2001) and for local, earthquake-generated tsunamis, determination of $\dot{n}(\mathbf{r}_0, \psi_s)$ becomes considerably more difficult.

A somewhat different approach has been proposed by Rikitake and Aida (1988). In this case, characteristic sources (relative to tsunami generation) are defined at eight zones along subduction zones bordering the Pacific coast of Japan. The tsunami wave height distribution along the Japan coast is calculated for each characteristic source:

$$h_{\max}(\mathbf{r}, \mathbf{r}_{\text{zone}}) \text{ zone } = 1, 2, \ldots, 8. \tag{3}$$

In each zone, the characteristic earthquake is assigned a 10-year probability (P_{eq} ($\mathbf{r}_{\text{zone}}$,T = 10 yr)), using both exponential (Equation 2) and Weibull distributions and based on a recurrence rate of $\dot{n}(M_{\text{char}})$. For each zone, the probability that tsunami amplitude h_{crit} will be exceeded in time T is given by

$$P(\mathbf{r}, \mathbf{r}_{\text{zone}}, h_{\text{crit}}, T) = \begin{cases} P_{\text{eq}}(\mathbf{r}_{\text{zone}}, T), & h_{\max}(\mathbf{r}) \geq h_{\text{crit}} \\ 0, & h_{\max}(\mathbf{r}) < h_{\text{crit}}. \end{cases} \tag{4}$$

The combined tsunami probability for n zones is

$$P(\mathbf{r}, h_{\text{crit}}, T) = 1 - \prod_{\text{zone}=1}^{n} [1 - P(\mathbf{r}, \mathbf{r}_{\text{zone}}, h_{\text{crit}}, T).] \tag{5}$$

In this approach, $\dot{N}(\mathbf{r}, h_{\text{crit}})$ is not explicitly calculated. As in PSHA, characteristic earthquake size distributions are often considered separately from G–R distributions, though Field *et al.* (1999) shows how these two distributions can be combined. One can also modify the Rikitake and Aida (1988) approach to consider a distribution of discrete earthquake magnitudes, each with an assigned G–R recurrence rate, rather than strictly considering only characteristic earthquakes.

2.2. UNCERTAINTIES

As discussed in Geist (2005), it is convenient to classify uncertainties associated with PTHA calculations according to the generation, propagation, and runup processes and whether the uncertainties are epistemic or aleatory (Senior Seismic Hazard Analysis Committee, SSHAC, 1997; Toro *et al.*, 1997; Anderson and Brune, 1999). In practice, most of the uncertainties associated with PTHA are epistemic in that collection of additional data decreases the level of uncertainty (e.g., higher resolution bathymetry improves the accuracy of numerical propagation computations, Matsuyama *et al.*, 1999). For a few parameters such as event-to-event variations in slip distribution, uncertainty is inherent in the physics of earthquake rupture (i.e. aleatory) and is not reduced by the collection of additional data. Another example of aleatory uncertainty is the tidal level at the time of tsunami arrival (Mofjeld *et al.*, 1997).

Tsunami source parameters with epistemic uncertainties can be incorporated in a logic-tree approach (Coppersmith and Youngs, 1986; Cramer *et al.*, 1996; Senior Seismic Hazard Analysis Committee, (SSHAC), 1997). For example, the maximum earthquake magnitude that any given fault can generate may be subject to different interpretations of, for example, fault length, seismogenic depth, and slip rate. More generally, different frequency–magnitude curves can be envisioned to conform to either a modified G–R relationship in which the b-value is greater for larger earthquakes (Pacheco *et al.*, 1992; Sornette and Virieux, 1992; Romanowicz and Rundle, 1993; Kagan, 1999; Pisarenko and Sornette, 2004) or a characteristic model for the largest earthquake (Wesnousky, 1994; Kagan, 2002b). If hazard analysis is based on the seismic moment ($M_0 = \mu\, LW\overline{D}$) of potential earthquakes, then values and associated uncertainties for first-order parameters such as rupture length (L), width (W), shear modulus (μ), and average slip ($\overline{D}$) must be provided. A number of theoretical and empirical scaling relationship linking the geometric and kinematic (i.e., $\overline{D}$ or static stress drop) parameters have been proposed (Kanamori and Anderson, 1975; Geller, 1976; Wyss, 1979; Scholz, 1982; Romanowicz and Rundle, 1993; Wells and Coppersmith, 1994; Somerville *et al.*, 1999; Shaw and Scholz, 2001; Miller, 2002). In addition, values for shear modulus are often taken from a standard reference earth model (Dziewonski and Anderson, 1981), though recent observations in subduction zones (Bilek and Lay, 1999, 2000) suggest that lower values near the surface may have a significant effect on tsunami generation (Geist and Bilek, 2001). Finally, other parameters that relate to fault zone geometry (dip, fault depth) have a significant effect on tsunami generation (Geist, 1999) – typically, these parameters are constrained by deep-crustal seismic imaging (e.g., Parsons *et al.*, 1998) and precise hypocenter locations (e.g., DeShon *et al.*, 2003).

An example of a simplified logic tree that accommodates epistemic uncertainty in three model parameters is shown in Figure 1. In this example, different seismogenic depths ($z_1 \cdots z_4$) that control the rupture width for large events are considered, dependent on the choice of the recurrence relation. In contrast in this example, only two choices for shear modulus are used, independent of the other parameters in the logic tree. The joint probability for each branch of the logic tree is shown on the right-hand side. For a realistic analysis of epistemic uncertainty associated with local tsunamis, the logic tree can become much more complicated than shown in Figure 1 and Monte Carlo methods that sample extensive logic trees may need to be employed (e.g., Petersen *et al.*, 2002).

For aleatory uncertainty such as associated with slip distributions, the uncertainty is typically incorporated directly into the rate calculations

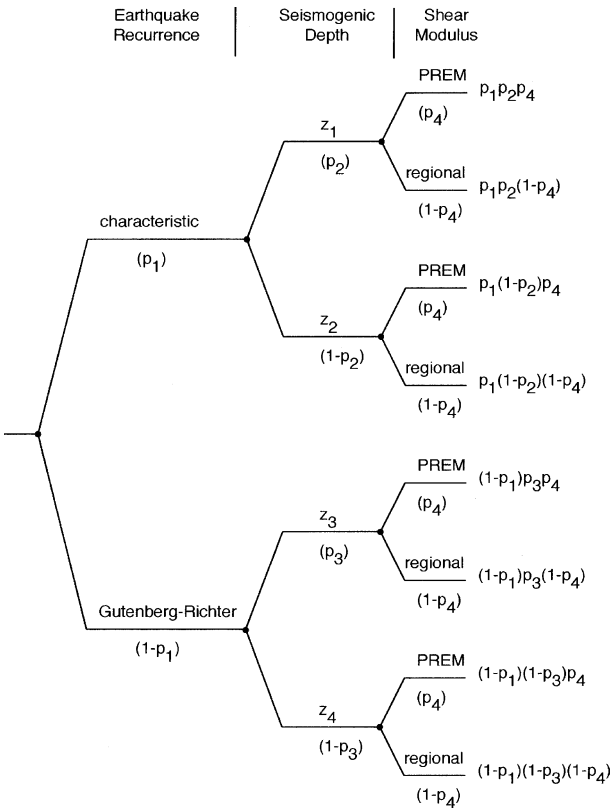

Figure 1. Example of a simplified logic tree for three model parameters: (1) earthquake recurrence (characteristic, Gutenberg–Richter), (2) seismogenic depths (z_1 ... z_4), and (3) shear modulus: PREM (Dziewonski and Anderson, 1981); regional observations (e.g., Bilek and Lay, 1999). For each parameter, the weighting factor is shown below in parentheses. Joint probabilities for each parameter shown on right-hand side.

(Equation 1). The cumulative probability (ϕ) that some hazard variable (Y) will be exceeded based on aleatory, normally distributed uncertainty is given by

$$\Phi(y \geq Y | \hat{Y}, \sigma_Y) = \int_Y^{\infty} \frac{1}{\sigma_Y \sqrt{2\pi}} \exp\left[-\frac{(y - \hat{Y})^2}{2\sigma_Y^2} \right] \mathrm{d}y, \tag{6}$$

where the expected value ($\hat{Y}$) and variance ($\sigma^2{}_Y$) are determined from regression analysis of existing data (Anderson and Brune, 1999). For PSHA, the natural logarithm of ground motion is the hazard variable with $\hat{Y}$ determined from empirical and theoretical attenuation relations that are a function of distance and magnitude ($\hat{Y} = f(r,m)$, $r = ||\mathbf{r} - \mathbf{r}_0||$) and $\sigma^2{}_Y$ determined from comparison to observations (Senior Seismic Hazard Analysis Committee, (SSHAC), 1997). Anderson and Brune (1999) assert, however, that a significant fraction of ground-motion uncertainty determined from attenuation relations is epistemic and should be handled in a different manner.) Then, the total exceedance rate is modified as follows:

$$\dot{N}(\mathbf{r}, Y) = \int \int \dot{n}(r, m) \Phi(y \geq Y | \hat{Y}, \sigma_Y) \mathrm{d}r \, \mathrm{d}m. \tag{7}$$

Aleatory uncertainty in the hazard variable for local tsunami amplitude ($h_{\max}$) mainly arises from the inherent variability in slip distribution during rupture. Unfortunately, there are few coastal locations where the expected value ($\hat{h}_{\max}(\mathbf{r}, m)$) and variance ($\sigma_h^2$) can be determined from empirical analysis of a sufficient number of earthquakes along a given fault. It is possible, however, that model-based values for $\hat{h}_{\max}(\mathbf{r}, m)$ and σ_h^2 can be derived through Monte Carlo analysis of a large number of slip distributions ($D(\xi,y)$ – ξ, y are coordinates resolved in the fault plane, Figure 2), such that

$$\hat{h}_{\max}(\mathbf{r}, m) = \frac{1}{N} \sum_i h_{\max}(\mathbf{r}, D_i(\xi, y, m)) \tag{8}$$

and

$$\sigma_h^2 = \frac{1}{N} \sum_i [h_{\max}(\mathbf{r}, D_i(\xi, y, m)) - \hat{h}_{\max}(\mathbf{r}, m)]^2. \tag{9}$$

The procedure for calculating tsunami amplitudes from a stochastic, slip-distribution model is discussed by Geist (2002). If $h_{\max}(\mathbf{r},D(\xi,y,m))$ for a particular coastal site and earthquake magnitude is normally distributed, then Equation (6) can be used to calculate the cumulative probability ϕ. An example of this method is given for the characteristic earthquake model in the Cascadia case study below. Similar methods

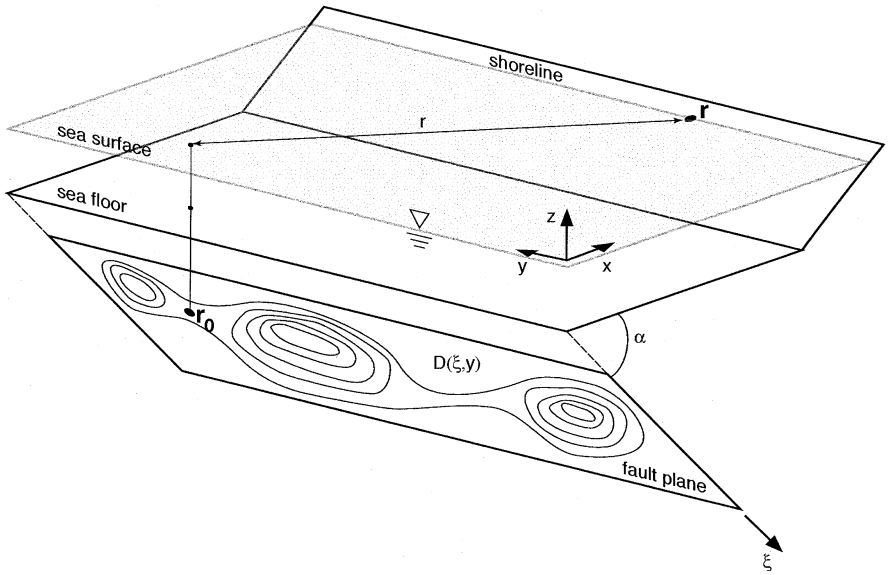

Figure 2. Geometry for local tsunamis generated by distributed slip ($D(\xi, y)$) along a dipping thrust fault. Position vectors shown for source location ($\mathbf{r}_0$) and shoreline location ($\mathbf{r}$). Modified from Geist and Dmowska (1999).

can be employed to account for uncertainty in when the tsunami occurs relative to the tidal stage.

2.3. MONTE CARLO SIMULATIONS

Monte Carlo techniques are useful for including multiple sources of uncertainty in hazard analysis (Savage, 1992; Cramer *et al.*, 1996; Ebel and Kafka, 1999). Monte Carlo or stochastic simulation (Rubinstein, 1981) involves using a large statistical sample in calculating initial conditions for a numerical model. To determine tsunami recurrence rates and probabilities, a seismic zonation scheme is developed based on fault structure and tectonics that can include both far-field and local sources (e.g., Ward, 1994; Kagan, 2002a). Within each zone, a random sample of earthquake magnitudes are chosen according to a modified G–R distribution with the epicenter randomized such that the rupture area does not extend outside the seismic zone. (In contrast, for the characteristic model earthquake magnitude and location are derived, in part, from fault segment boundaries defined *a priori*.) In addition, for each earthquake a stochastic slip distribution is used to calculate the initial conditions for tsunami propagation (Geist, 2002). Other parameters that are typically taken to be constant are fault plane geometry, shear modulus, and a constant scaling relationship between seismic moment and the length and width dimensions of rupture.

The Monte Carlo simulation is based on selecting a random sample of earthquake magnitudes from the modified G–R distribution of Kagan and Jackson (2000) (see also Vere-Jones *et al.*, 2001). For a lower-magnitude cutoff (M_t) that represents catalog completeness and an upper-magnitude corner (M_c) that fixes the tail of the distribution, the cumulative distribution is given by

$$F(M) = (M_t/M)^{\beta} \exp[(M_t - M)/M_c], \tag{10}$$

where the exponent β is related to the b-value of the G–R distribution according to $b = (3/2)\ \beta$ (Kagan, 1997, 1999). An example of a modified G–R distribution is plotted in Figure 3 for $M_t = 7.0$ and $M_c = 9.0$ (dashed line) along with a the cumulative distribution of 100 random samples taken from Equation (10) (medium solid line). As a measure of variability of this random sample, we also plot the envelope of 20 sets of 100 random samples (two light solid lines) (cf., Field *et al.*, 1999). Increasing the number of

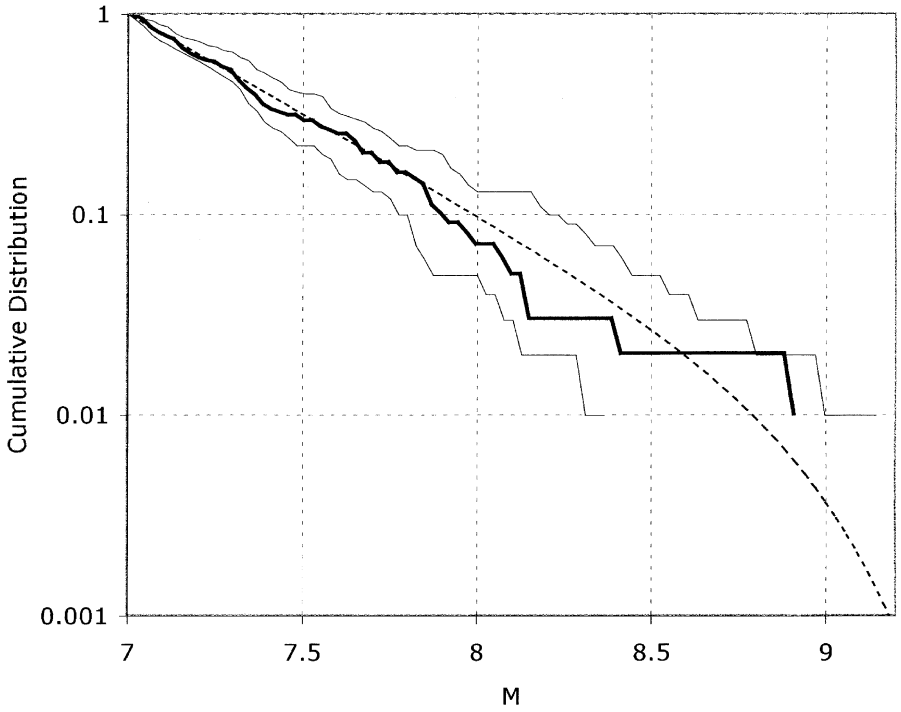

Figure 3. Cumulative distribution function (dashed line) for the modified Gutenberg–Richter relationship given by Kagan and Jackson (2000) and Vere-Jones *et al.* (2001). Cumulative number of earthquakes from 1 set of $N = 100$ random samples according to this distribution shown by medium solid line. Envelope of 20 sets of $N = 100$ random samples per set shown by the two light solid lines.

random samples decreases the variability caused by sampling (as measured by the envelope), but increases the computational cost if these samples are used in tsunami simulations. One can determine the average return time of earthquakes of magnitude M_w, and greater based on a geologic-based estimate of the seismic moment budget for the entire seismic zone ($\dot{M}_{geol}^{zone}$) as indicated by Ward (1994):

$$\dot{M}_{geol}^{zone} = \mu L H_s \dot{s}_{geol}, \tag{11}$$

where L is the length of the seismic zone, H_s is the seismogenic width, and $\dot{s}_{geol}$ is the fault slip rate. This estimate implicitly assumes that the seismic coupling coefficient (χ) equals 1 through the seismogenic zone. Kagan (2002a) gives expressions to determine the activity rate (i.e. yearly number of earthquakes greater than a threshold magnitude) for different distributions such as Equation (10).

Once we have a random sample of earthquake magnitudes based on a physically realistic distribution, the rupture length and width (L, W) for tsunami generation can be determined from scaling relationships. The average amount of slip ($\overline{D}$) that constrains the scaling of the stochastic slip distribution is then determined from the geometric parameters and shear modulus (μ) according to

$$M_0 = \mu L W \overline{D}. \tag{12}$$

The choices for scaling relationships are subject to interpretation; multiple scaling relationships could be used to determine a level of epistemic uncertainty. Finally, for each earthquake epicenter, magnitude, and slip distribution, the tsunami propagation model is run to determine the tsunami amplitude or runup along the coastline from sources in each defined seismic zone.

3. Analysis of Empirical Tsunami Data

It has been shown in previous studies (Soloviev, 1969; Houston *et al.*, 1977; Horikawa and Shuto, 1983; Burroughs and Tebbens, 2005) that at a given coastal location, tsunami amplitudes follow a definable frequency-size distribution over a sufficiently long amount of time. For regions with an extensive catalog of observed tsunami wave heights, this method can be of great use in establishing tsunami probabilities. Accurate determination of the scaling constants, however, depends on a number of factors, including number of observations, measurement range of observations, and catalog completeness. In this section, different mathematical forms for the scaling relationship are reviewed, followed by how the aforementioned factors affect the probability calculations and how empirical analysis has been used on a region-wide basis in the past.

The frequency-size distribution introduced by Soloviev (1969) is of the form

$$\dot{n}(i) = \alpha_1 10^{-\beta_1 i}, \tag{13}$$

where α_1 and β_1 are constants, $\dot{n}$ is the number of events per annum, and i is tsunami intensity calculated from the average runup (h_{avg}) along a stretch of coastline:

$$i = \log_2(\sqrt{2h_{\text{avg}}}). \tag{14}$$

Rather than use tsunami intensity, for the analysis of Hawaiian tsunamis Houston *et al.* (1977) used the maximum elevation of tsunami waves 200 ft. inland of the coast (h_{200}):

$$\dot{n}(h_{200}) = \alpha_2 10^{-\beta_2 h_{200}}. \tag{15}$$

In addition, for the analysis of tsunami source regions along the Alaska and Peru-Chile subduction zones, Garcia and Houston (1975), Houston (1980), and Crawford (1987) used an exponential frequency-size distribution of the form

$$\dot{n}(i) = \alpha_3 \mathrm{e}^{-\beta_3 i}. \tag{16}$$

More recently, Burroughs and Tebbens (2005) proposed that tsunami runup heights follow a power-law relationship similar to many other natural systems, particularly the Gutenberg–Richter frequency–magnitude relationship for earthquakes. In examining extensive records of tsunami wave heights at several locations in Japan, they conclude that the cumulative frequency-size distribution is best fit by a power-law relationship of the form

$$\dot{n}(h) = Ch^{-\alpha_4}, \tag{17}$$

where h is the maximum tsunami height recorded at a single site (U.S. National Geophysical Data Center tsunami catalog). At some sites, the catalog data are best fit by an upper-truncated power-law (Burroughs and Tebbens, 2001):

$$\dot{n}_r(h) = C(h^{-\alpha_4} - h_U^{-\alpha_4}), \tag{18}$$

where h_U is the wave height where the frequency falls to zero. Burroughs and Tebbens (2001, 2005) explain that the upper-truncated power law is a result of either temporal limitations (large events not included in the catalog) or physical bounds on the phenomenon at a particular site (e.g., wave breaking prior to runup). If we assume that the inter-event arrival times and magnitudes are independent, characteristic of a Poisson process as in PTHA (Equation 2), then the cumulative distribution function is given by

$$P(h \geq h_{\text{crit}}) = 1 - \mathrm{e}^{-\dot{n}(h_{\text{crit}})T}, \tag{19}$$

where h_{crit} is the wave height of interest or risk tolerance and T is the time period of interest or exposure time. As noted by Houston *et al.* (1977), for example, the probability in a 10 or 50-year time frame that a 1-in-100 year wave height would occur is not insignificant: $P = 0.10$ and 0.39, respectively.

Probabilistic assessment of tsunami hazards using an empirically derived frequency-size distribution is dependent on how well the distribution is constrained by the catalog data. First, Horikawa and Shuto (1983) show that the average frequency of a tsunami of intensity equal to or greater than that of the 1896 Sanriku tsunami ($i \geq 4$) is 0.005 yr^{-1} (1 in 200 year event) if an exponential function is used, versus 0.01 yr^{-1}(1 in 100 year event) if a power-law distribution is used. The choice of distribution is obviously important in estimating the recurrence rate of tsunamis. For river floods also, Malamud *et al.* (1996) shows that the standard log-Pearson Type III distribution (U.S. Interagency Advisory Committee on Water Data, 1982) and power-law distribution yield significantly different recurrence rates. The power-law distribution may be preferable in most cases (Malamud *et al.*, 1996). Recent research has also shown that many other physical phenomena follow a power-law frequency-size distribution (e.g., Ito and Matsuzaki, 1990; Birkeland and Landry, 2002; Malamud *et al.*, 2004). In addition to the form of the scaling relationship used (i.e., exponential, power-law), Burroughs and Tebbens (2005) provide two criteria to determine whether a particular frequency-size distribution can be used for probabilistic forecasting: (1) the scaling exponent (α) should be the same for both short and long time intervals and (2) the scaling relationship from the data excluding the largest events in the catalog should be consistent with those largest events. For cases where a best-fit upper-truncated power law is caused by an incomplete catalog missing large events, Burroughs and Tebbens (2005) indicate that a power-law relationship should be used for probabilistic assessments. Catalog completeness is an important factor to evaluate, especially with respect to the types of measurements being made (runup measured by post-event surveys versus tsunami amplitude recorded at tide-gauge stations), the accuracy of the measurements, and the range of tsunami wave height recorded. The latter often varies historically, with the development and deployment of tide-gauge stations and other instruments as will be evident in the Acapulco case study below.

Because empirical frequency-size distributions are derived from historical records at a given site, several schemes have been developed to perform a regional hazard assessment using these distributions. To calculate the frequency of occurrence of tsunami waves for the Hawaiian Islands, Houston *et al.* (1977) first determined the frequency-size distributions at locations

where historical data is available (e.g., Hilo, Honolulu). At locations where historical data are unavailable, they calculated a relative response function using a finite-element hydrodynamic model, calibrated using large past events (e.g., 1960 Chile and 1964 Alaska tsunamis). In this way, they were able to interpolate the empirical constants region wide. This method was modified to determine the frequency of occurrence for tsunamis along the west coast of the United States (Garcia and Houston, 1975; Houston, 1980). In this case, frequency-size distributions were established for far-field source regions in Alaska and Peru-Chile. Using some simplifying assumptions regarding tsunami generation, tsunami wave heights were calculated in central and southern California and Puget Sound for a range of tsunami intensity values and associated frequency of occurrence values. This approach, however, ignores possible tsunamis generated locally and from other far-field source regions.

4. Acapulco Case Study

For the first case study, a site-specific hazard analysis is introduced using primarily empirical analysis. A Monte Carlo simulation of local tsunamis is also performed to indicate where the tsunami catalog may be incomplete. Acapulco, Mexico (Figure 4) is chosen primarily because of the length of the historic tsunami record and the high rate of seismic activity along the southern Mexico subduction zone. A tsunami catalog is compiled from previous sources (Iida *et al.*, 1967; Soloviev and Go, 1984; Sanchez and Farreras, 1993) to determine an empirical cumulative frequency–runup relationship. This is compared to a synthetic cumulative frequency–runup relationship determined from a Monte Carlo simulation for local earthquakes.

The tsunami catalog listed in Table I and shown on Figure 5 is based primarily on the work of Sanchez and Farreras (1993), who have listed descriptions of each event along with tide gauge records where available. Eighteenth to early 20th-century observations are made from visual accounts. Runup estimates often refer to wave heights as tsunamis impinge on landmarks and structures, relative to mean sea level or normal high-water marks. Late 20th-century tsunami observations are from the tide gauge network that was installed in 1952 (Sanchez and Farreras, 1993) (though a tide gauge reading is referred to for the 12/14/1950 tsunami).

The two different types of observations present some difficulties in constructing a uniform catalog. This is evident in Figure 5 where the installation of the tide gauge network resulted in more frequent, low-runup observations. The visual estimates are subject to a large degree of error, perhaps as large as 1–2 m. The tide gauge measurements record wave

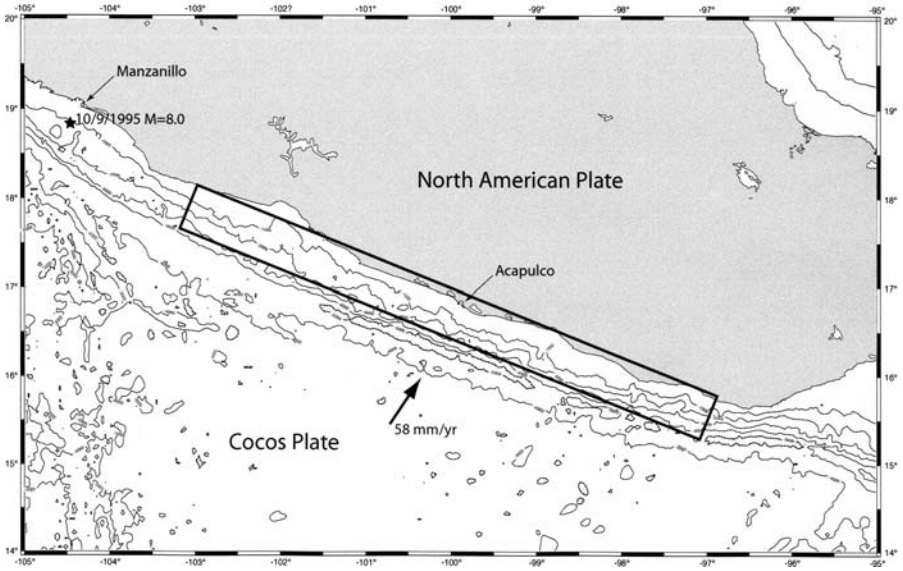

Figure 4. Bathymetric map offshore southern Mexico (contour interval: 1000 m). Rectangle represents seismic zone along interplate thrust for Monte Carlo tsunami simulation. Arrow: relative plate convergence vector (Cocos-North American plates).

amplitudes more accurately, although in a protected harbor subject to the effects of resonance and not runup on the open coast *per se*. Therefore, an assumption needs to be made to convert the amplitude measurements to runup values. The dynamics of tsunami runup depend on a number of factors in addition to the offshore wave amplitude, including wave polarity, leading wave steepness, and bathymetric slope (Tadepalli and Synolakis, 1996). As an example of how these two tsunami measurements compare, we can look at the data available for the 1995 Colima-Jalisco tsunami recorded near Manzanillo, Mexico (Figure 4). The post-tsunami runup survey indicates that runup on the open coast nearest Manzanillo was 4.75 m decreasing to 1.75 m along the beach to the south (Borrero *et al.*, 1997). In contrast, the tide gauge measurement inside Manzanillo harbor indicates that the maximum amplitude is approximately 1.0 m with a peak trough-crest wave height of approximately 2.2 m (Ortiz *et al.*, 2000). For the case of the Acapulco catalog, we simply assume that the peak trough-crest height reported by Sanchez and Farreras (1993) is the runup height. A more complete calibration would require detailed inundation modeling including overland flow. Even so, observations that pre-date the tide gauge network are in different locations near Acapulco; variability in observation location itself may cause inconsistencies in runup as was observed for the 1993 Hokkaido tsunami (Titov and Synolakis, 1997).

Table I. Tsunami events at Acapulco, Mexico with reported runups.

Date	Source location	Max. runup (m)	Measurement type	References
2/25/1732	Local	4	Visual estimate	Sanchez and Farreras (1993)
9/1/1754	Local	5	Visual estimate	Sanchez and Farreras (1993)
3/28/1787	Local	8	Visual estimate	Sanchez and Farreras (1993)
5/4/1820	Local	4	Visual estimate	Sanchez and Farreras (1993)
5/9/1877	N. Chile	1	Visual estimate	Sanchez and Farreras (1993), NGDC
4/14/1907	Local	2	Visual estimate	Sanchez and Farreras (1993), NGDC
7/30/1909	Local	9	Visual estimate	Iida *et al*. (1967), Soloviev and Go (1984), NGDC
12/14/1950	Local	0.3	Tide gauge	Sanchez and Farreras (1993), NGDC
11/4/1952	Kamchatka	0.5	Tide gauge (?)	Iida *et al*. (1967), NGDC
3/9/1957	Aleutians	0.64	Tide gauge	Sanchez and Farreras (1993)*
7/28/1957	Local	2.60	Tide gauge	Sanchez and Farreras (1993)*
5/22/1960	Chile	1.92	Tide gauge	Sanchez and Farreras (1993)*
11/20/1960	Peru	0.13	Tide gauge	Sanchez and Farreras (1993)*
5/11/1962	Local	0.81	Tide gauge	Sanchez and Farreras (1993)*, NGDC
5/19/1962	Local	0.34	Tide gauge	Sanchez and Farreras (1993)*
10/13/1963	Kurile Islands	0.49	Tide gauge	Sanchez and Fafferas (1993)*
3/28/1964	Alaska	1.07	Tide gauge	Sanchez and Farreras (1993)*
2/4/1965	Aleutians	0.40	Tide gauge	Sanchez and Farreras (1993)*
8/23/1965	Local	0.40	Tide gauge	Sanchez and Farreras (1993)*, NGDC
1/14/1966	Local	0.40	Tide gauge	NGDC
5/16/1968	Japan	0.43	Tide gauge	Sanchez and Farreras (1993)*
1/30/1973	Local	0.43	Tide gauge	Sanchez and Farreras (1993)*
11/29/1975	Hawaii	0.34	Tide gauge	Sanchez and Farreras (1993)*
1/14/1976	Kermadec Islands	0.24	Tide gauge	Sanchez and Farreras (1993)*
3/14/1979	Local	1.31	Tide gauge	Sanchez and Farreras (1993)*
12/12/1979	Colombia	0.30	Tide gauge	Sanchez and Farreras (1993)*, NGDC
10/25/1981	Local	0.09	Tide gauge	Sanchez and Farreras (1993)*, NGDC
9/19/1985	Local	1.15	Tide gauge	Sanchez and Farreras (1993)*
9/21/1985	Local	1.20	Tide gauge	Sanchez and Farreras (1993)*, NGDC

NGDC: Online tsunami runup database from the National Geophysical Data Center (URL: http://www.ngdc.noaa.gov/seg/hazard/tsu.shtml).
*Maximum runup from tide gauge records is assumed to be the maximum crest-trough height as reported by Sanchez and Farreras (1993).

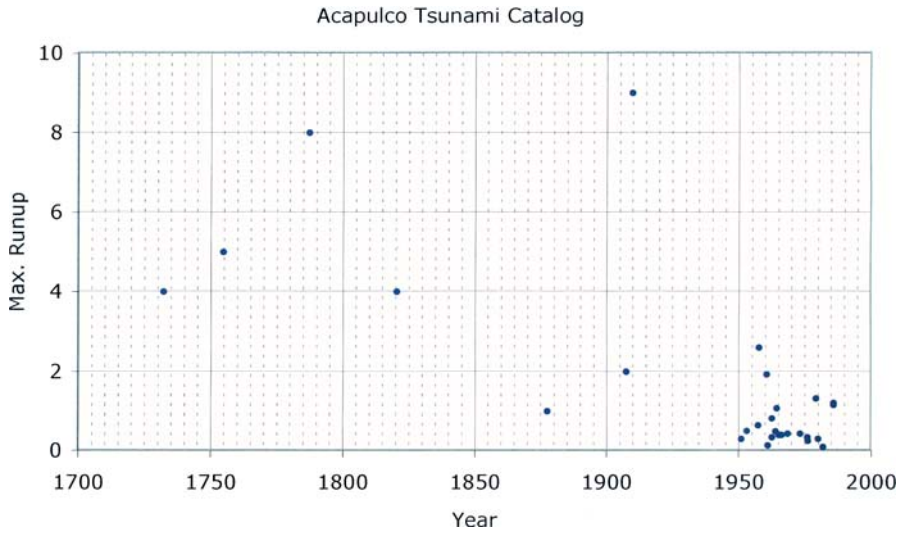

Figure 5. Tsunami catalog for Acapulco, Mexico. Higher density of measurements starting in 1952 corresponds to installation of regional tide gauge network (Sanchez and Farreras, 1993).

Despite the difficulties in constructing a tsunami catalog for Acapulco, a fairly well-defined cumulative frequency–runup relationship is evident from the data (Figure 6). An empirical best-fit trend is shown in Figure 6 based on all measurements >0.1 m using the upper-truncated power-law relationship (Equation 18). Figure 6a shows the trend line for all of the available data spanning the time period of 1732–1996, whereas Figure 6b shows only the tide gauge data from 1950–1996. In comparing the figures, the empirical analysis of just the tide-gauge data (Figure 6b) yields accurate recurrence rates for tsunamis less than approximately 3 m. Because of a lack of information for small tsunami for the entire catalog, Figure 6a indicates artificially low recurrence rates for small tsunamis. This is consistent with the display of tsunami events shown in Figure 5 where no events <1 m were recorded 220 years prior to the installation of the Acapulco tide gauge ($\sim$80% of the catalog duration). However, empirical analysis of just the tide-gauge data yields no constraint on the frequency of large tsunamis as in Figure 6a.

A Monte Carlo simulation was performed to predict the cumulative frequency–runup curve for Acapulco as described in the section above. Several authors have noted the shallow depth of the seismogenic zone for the Mexican interplate thrust (Suárez *et al.*, 1990; Tichelaar and Ruff, 1993; Suárez and Sánchez, 1996), indicating a narrow potential rupture width compared to many other continental subduction zones. This limits the maximum magnitude along the subduction zone to M = 8–8.5 (Singh

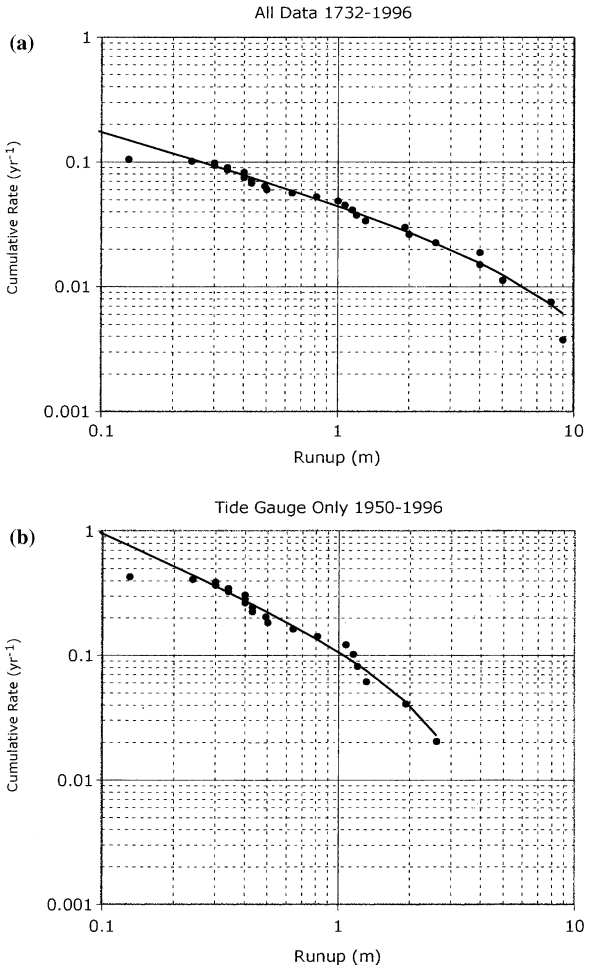

Figure 6. Cumulative rate of tsunamis (yr^{-1}) that exceed the runup value given by the abscissa for the Acapulco tsunami catalog. (a) All local and far-field tsunami observations (1732–1996). Trend line fit by upper-truncated power law ($C = 0.056$, $\alpha_4 = 0.52$, $h_U = 20$ m). (b) Only tide gauge recordings of local and far-field events (1950–1996) ($C = 0.16$, $\alpha_4 = 0.81$, $h_U = 4.2$ m).

et al., 1983; Ward, 1991, 1992; Suárez and Sánchez, 1996). A single seismic zone is considered such that $L = 720$ km and $W = 60$ km (Figure 4). The seismic moment release rate is determined assuming a fault slip rate of 58 mm/yr and $\chi = 1$ (Equation 11). Geometry of the Mexican interplate thrust is taken from seismicity and controlled source, wide-angle seismic refraction studies (Valdes *et al.*, 1986; Suarez *et al.*, 1990). Two hundred earthquakes were chosen from a random sample of the modified G–R distribution (Equation 10) with $M_t = 7.0$ and $M_c = 8.0$ (the latter corresponding to $M_{max} = 8.0 \pm 0.1$ in Ward, 1991). Although a simple distribution is

used in this modeling exercise, Singh *et al.* (1983) and Ward (1991, 1992) note a non-constant *b*-value for seismicity in this region with a noticeable concentration of earthquakes near M = 7–7.5. The rupture length is derived from M_w based on a empirical relationship determined by Wells and Coppersmith (1994). For rupture width less than $W = 60$ km, an aspect ratio of 2:1 is assumed (Geller, 1976); otherwise the rupture width is fixed at $W = 60$ km. Randomizing the epicentral location within the defined seismic zone and using slip distributions from the stochastic source model, peak nearshore tsunami amplitude (PNTA) values are computed from the tsunami propagation model. PNTA at Acapulco as a function of earthquake magnitude is shown in Figure 7. Although the trend of increasing PNTA with earthquake magnitude is apparent, there is substantial scatter in the model results, owing primarily to the effects of varying propagation distance and direction.

We compare the cumulative frequency–runup curve from the Monte Carlo simulation to that for the local tsunami catalog data in Figure 8. As in Figure 6, a best fit upper-truncated power-law relationship is fit to the local data (dashed line). To convert the PNTA values to equivalent runup values, an amplification factor of 2 is assumed that is typical of threshold propagation models of the type used in this simulation (i.e., models where propagation computations are stopped at a specific isobath) (Shuto, 1991; Imamura *et al.*, 1993). In general, small shifts in the computationally based frequency–runup curve would occur by assuming different values for the seismic moment release rate (shifts along the ordinate) or for the amplification factor in the threshold modeling (shifts along the abscissa). In addition, the tail of the frequency–runup curvey is controlled by the choice of

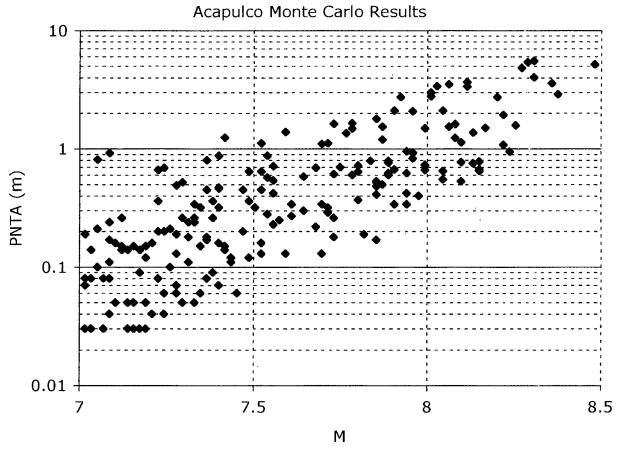

Figure 7. PNTA at the latitude of Acapulco computed from a Monte Carlo simulation using 200 earthquakes (M7–8.5).

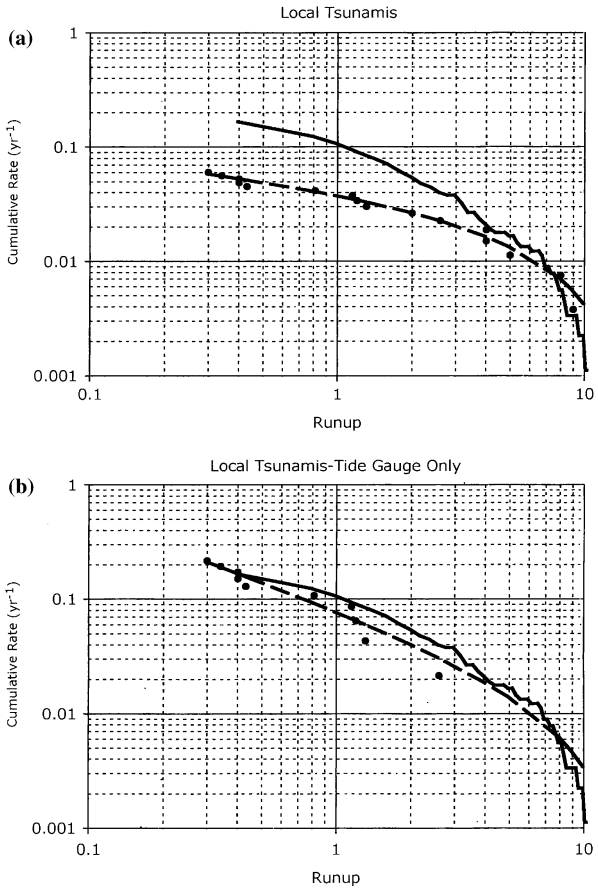

Figure 8. Comparison of cumulative frequency–runup curves from the tsunami catalog (dashed line) using only the local events (dots) with exceedance rate curve computed from Monte Carlo simulation (solid line). (a) All local tsunami observations (1732–1996). Discrepancy between the two curves likely omplete low-runup observations in the tsunami catalog prior to 1950. (b) Only tide gauge recordings of local events (1950–1996).

M_c for the earthquake distributions input to the tsunami model. The deviation between the Monte Carlo simulation and empirical curves using all the local tsunami observations (Figure 8a) indicates the importance catalog completeness has on the empirical results. The higher rate of low-runup tsunamis (0.1–2 m) predicted by the simulation compared to empirical analysis confirms that the portion of the tsunami catalog that predates the installation of the tide gauge network is incomplete in this runup range. If we only use tide gauge recordings of local tsunamis in the empirical analysis, we observe a much better agreement with the computational results (Figure 8b). However, we also note that the tail of the cumulative

frequency–runup curve is better constrained using the entire local dataset (Figure 8a). The primary use of computational methods in this case study is to indicate areas where empirical analysis for different datasets is deficient.

5. Cascadia Case Study

For the second case study, a region-wide analysis of the Cascadia margin coastline is formulated primarily using Monte Carlo simulation. Empirical analysis of the existing data in this case is used to determine background probabilities of tsunamis from far-field sources. PTHA for local tsunamis is then discussed in terms of both a characteristic model and, as with the Acapulco case study, a modified G–R model. It should be noted, however, that these two models (characteristic and G–R) can be combined as demonstrated by Field *et al.* (1999) for seismic hazard analysis.

5.1. EMPIRICAL ANALYSIS

Since the 1850's, nine Pacific-rim earthquakes have caused ≥1 m run up in 69 separate incidents along the U.S Pacific coast (Figure 9). At least 16 deaths and ~8.3 M in damage are attributable to far-field tsunamis that struck California, Oregon and Washington (source: National Geophysical Data Center). These tsunamis originated from all around the Pacific rim: Chile, Hawaii, Japan, the Kuril trench, and Alaska.

At any given point along the U.S. West Coast, there is an insufficient record to develop a cumulative-frequency–runup distribution as was done for Acapulco. However, a region-wide analysis of empirical data that calculates a frequency above a threshold runup can be calculated. The region-wide catalog shown in Figure 9 allows us to calculate a far-field tsunami frequency at a variety of sites along the U.S. Pacific coast. Since there are at least five major sources of far-field tsunamis, their occurrence is treated as random in time, and the observed frequencies are used in a Poisson probability model built around an exponential distribution as in Equation (2). The odds of a far-field tsunami strike can be pre-calculated and treated as the background probability for a given area of interest. The probability of locally sourced events can be superimposed over the background probability using Equation (5).

We generated a set of far-field tsunami probability calculations for the continental U.S Pacific coast (Figure 10). We divided the coast into ~100-km zones (measured by latitude) and tallied the number of far-field tsunami events with recorded run up ≥1 m. From these patterns, inter-event times can be estimated for each 100-km bin by using observed time differences between events and the open intervals at the beginning and end of the 1854–2004 observation period. To account for the open inter-

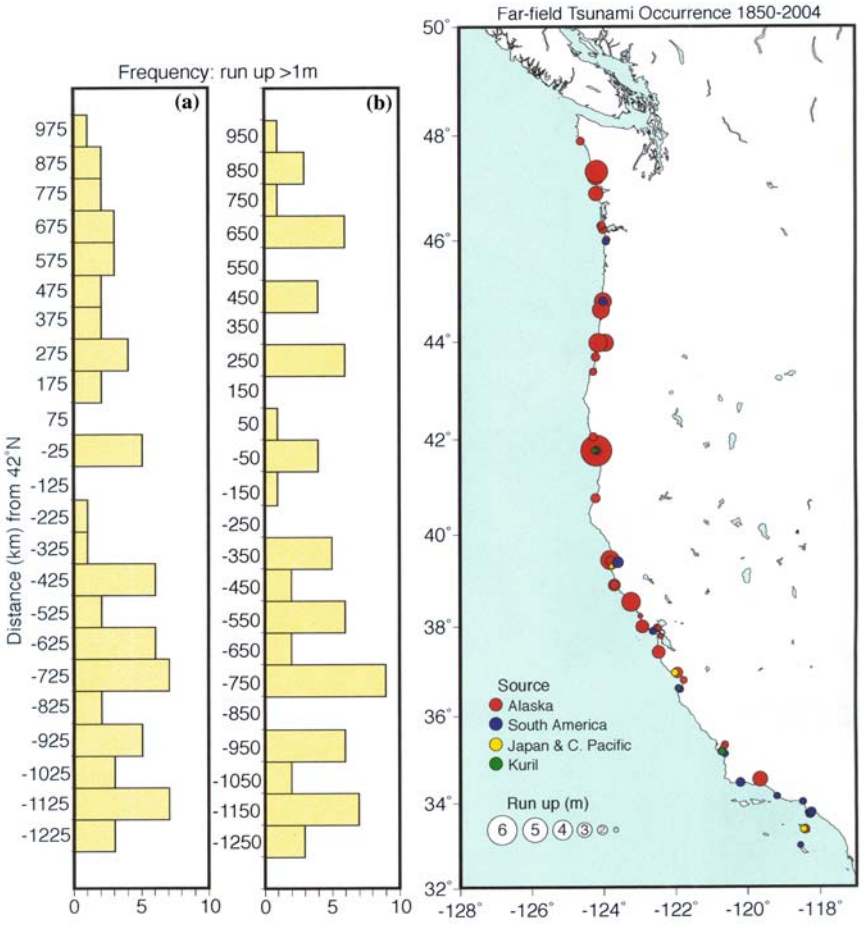

Figure 9. Observations of ≥1 m run up caused by far-field tsunamis along the continental U.S. Pacific coast. Circles are scaled by runup magnitude, and colored according to source region. Two different histograms of far-field tsunami frequency are shown; in both cases the frequencies are calculated using ~100 km bins. The difference between the two plots is that the bin boundaries are uniformly shifted by 25 km to show the effects of different bin locations. The frequencies shown were modeled with a Monte Carlo method to account for open intervals on either end of the ~150-year observation period (see text) and used to calculate Poisson probability.

vals, inter-event times for fault segments were calculated using a Monte Carlo technique. Tsunami times were repeatedly drawn at random from exponential distributions of varying means (1–300 years) over a 500-yr period; distributions that could reproduce observed tsunami event times for bin within the last 150-yr part of the sequence were tracked, and the mean of all distributions that fit the observations was used in the recurrence models.

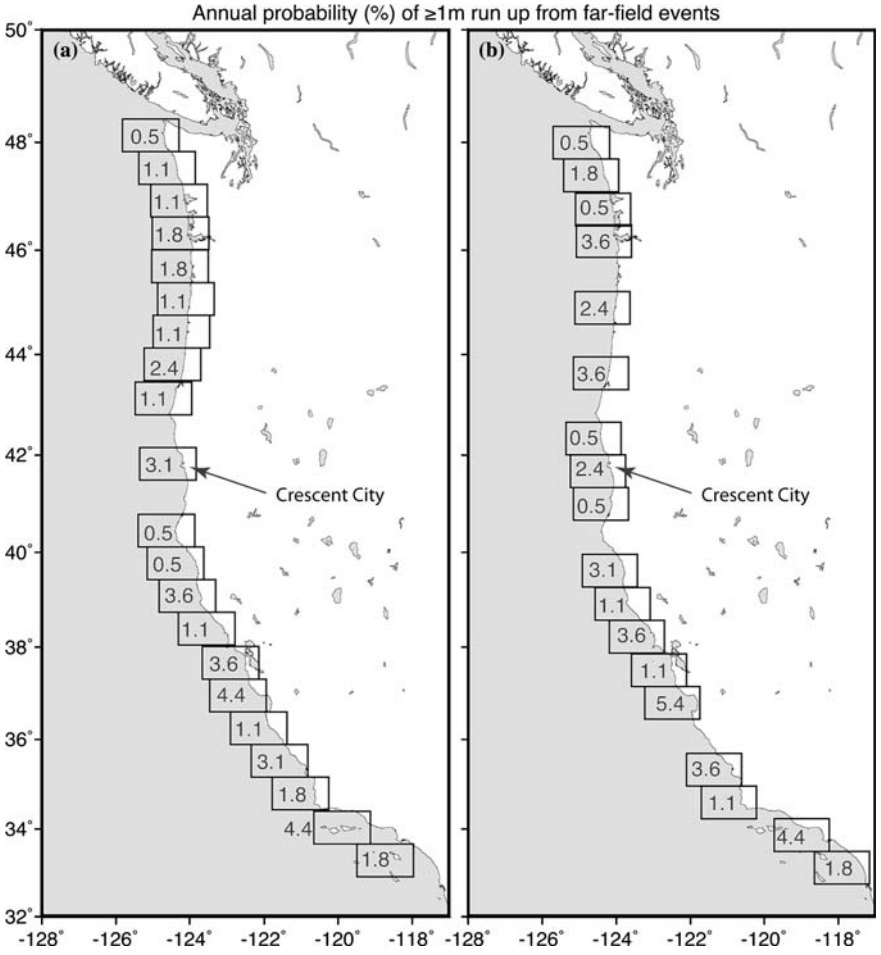

Figure 10. Two examples of Poisson probability calculations using the binning shown in Figure 9. These plots indicate the annual probability of ≥1 m run up caused by far-field tsunamis based strictly on empirical analysis. Note that the results are dependent on the bin locations (''a'' and ''b'' correspond to the same-labeled histograms in Figure 8). These values could be treated as background probability upon which the probability from local events is superimposed.

Use of a spatial binning technique for far-field tsunami probability causes the results to depend in part on the choice of the bin width and boundaries. Larger bins will have greater frequencies and higher probability. In addition, the locations of bin boundaries can have an effect (compare Figure l0a with b) because the observations are not uniformly distributed along the coast (see Figure 9). For ~100-km-long coastal areas along the continental U.S. Pacific coast, in general we find that the annual probability of ≥1 m run up from far-field tsunamis can range from ~1 to ~5% (Figure 10). Despite the

variability in runup probability caused by data availability and binning, in some areas such as near Crescent City, California, increased runup probability can be traced to physical sources – namely the nearshore hydrodynamic response to tsunamis as discussed by González *et al.* (1995).

5.2. CHARACTERISTIC EARTHQUAKES

For local Cascadia tsunamis, we first examine a scenario in which the interplate thrust along the Cascadia subduction zone only ruptures in characteristic $M=9$ earthquakes (i.e., characteristic earthquakes in terms of first-order source parameters, but not in terms of slip distribution) (Figure 11). This case provides an example of how the cumulative probability can be calculated for inherent variability in slip distribution patterns. The cumulative probability in this case is conditional upon an event with a set of source parameters (ψ_{M9}) occurring. The first-order source parameters (geometry, magnitude, average slip) for this case are based on the recent analysis of the 1700 ce earthquake and tsunami by (Satake *et al.*, 2003), using their "Long-Wide" rupture model. Results from the Long-Narrow model are discussed in Geist (2005). One hundred different slip distributions are generated using the stochastic source model and PNTA is calculated using a linear-long wave tsunami propagation model. Shown in Figure 11a is the mean and the ± 1 standard deviation lines for the suite of 100 stochastic ruptures for points along the coastline between latitudes 41° N and 48° N. Tsunami amplitudes are generally higher broadside from the center of the rupture zone (43°–46° N) because of the source radiation pattern (Ward, 1982) combined with nearshore wave propagation effects. Histograms are also shown for three locations to demonstrate the variability in PNTA distributions. (Green line represents a normal distribution given the mean and standard deviation of the amplitudes from the 100 ruptures). The right-hand graph shows the cumulative probability that PNTA $\geq$ 7 m given that this event will occur ($\phi(PNTA \geq 7 \text{ m} \mid \psi_{M9})$) calculated in two ways. The magenta line is based on calculations assuming a normal distribution (Equation 6). The cyan line is based on discrete summation of the model results. To calculate the total exceedance rate, one would multiply ϕ with the corresponding recurrence rate and integrate over all other source locations and magnitudes (Equation 7). If the average recurrence rate of these events is $1/520$ yr^{-1} as determined from coastal subsidence (e.g., Atwater and Hemphill-Haley, 1997), then hazard curves can be calculated for individual sites as shown in Figure 12 (labeled P). These hazard curves are constructed for a 520 year exposure time ($T=1$ avg. earthquake cycle) and are compared to the cumulative probability curves (ϕ) if the earthquake were to occur. This comparison emphasizes the fact that for a Poisson process and $\dot{N}T = 1$, P approaches $1 - e^{-1} \approx 0.63$ for

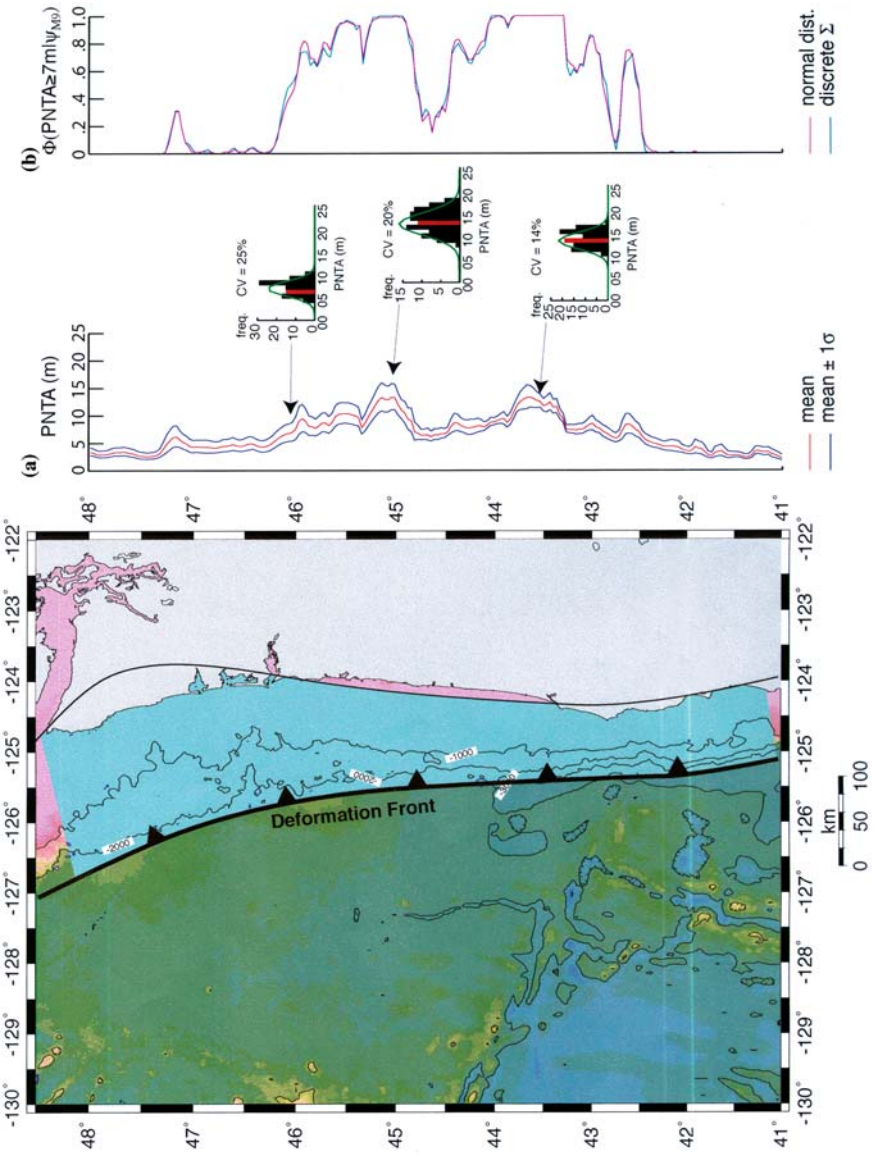

Figure 11. (Left) Map showing regional bathymetry and Cascadia interplate thrust. Light blue region represents example rupture area for a $M = 9$ earthquake bounded in the downdip direction by the 450 °C isotherm (Hyndman and Wang, 1994). (a) Mean and $\pm 1\ \sigma$ values of PNTA calculated using hydrodynamic simulations for 100 different slip distribution patterns (Geist, 2005). PNTA histograms shown at three locations with equivalent normal distribution (green line). (b) Cumulative probability that PNTA will exceed 7 m, given that the earthquake were to occur. Magenta line: calculated assuming normal distribution (Equation 6). Cyan line: calculated from discrete summation of model results. CV = coefficient of variation.

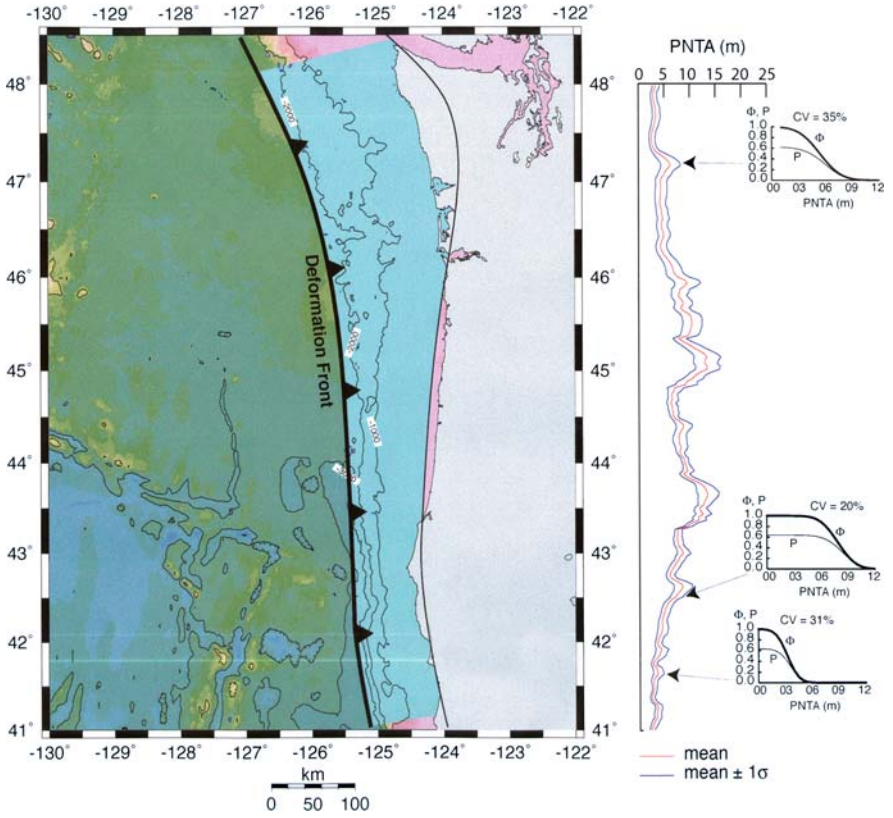

Figure 12. (Left) Map of $M = 9$ Cascadia rupture as in Figure 10. (Right) Mean and $\pm 1\ \sigma$ values of PNTA and hazard curves (thin line) for $\dot{N}T = 1$ assuming earthquake follow a Poisson process. For comparison, cumulative probability curves ((D) given that the earthquake were to occur are also shown. CV = coefficient of variation.

low PNTA values, whereas $\phi \rightarrow 1$. In contrast, for PNTA values that have a low exceedance probability, $P \approx \phi$ when $\dot{N}T = 1$. It should be noted that different recurrence rates have been determined from dating offshore turbidites (Adams, 1990; Goldfinger *et al.*, 2003). Also, different characteristic earthquakes have been employed such as with the National Seismic Hazard Maps that assume two weighted scenarios: (a) a $M = 9$ rupture with a recurrence interval of approximately 500 years and (b) a series of floating $M = 8.3$ earthquakes that fill the Cascadia seismic zone every 500 years (Frankel *et al.*, 1996, 2002).

5.3. GUTENBERG–RICHTER DISTRIBUTION

A contrasting earthquake model to the characteristic example above is to assume that earthquake magnitudes follow a G–R distribution. As in the Acapulco example, we consider a single seismic zone coincident with the

$M = 9$ rupture zone shown in Figure 11. The cumulative number of earthquakes per year as a function of magnitude derived from the distribution shown in Figure 3 is shown in Figure 13, assuming $L = 720$ km, $H_s = 120$ km, $\dot{s}_{geol} = 40$ mm/yr, $M_c = 9.0$, and $\chi = 1$. For a given location along the coastline (in this case, at 43.5° N), if PNTA is plotted as a function of earthquake magnitude (Figure 14a), considerable variability of tsunami amplitude is readily apparent for earthquakes in the range M = 7–8. This is primarily caused by the variability in propagation distance and direction for small earthquakes in the large defined seismic zone. If instead the maximum PNTA in the entire seismic zone for each earthquake is plotted as a function of magnitude (Figure 14b), then this variability decreases. The maximum PNTA is typically recorded closest to the rupture area (specifically, region of maximum slip) and thus statistics for the zone as a whole reduces variability in propagation distances. The cumulative frequency–PNTA curves are shown in Figure 15 for a single site and for the entire zone. These curves approximately follow a power-law relationship, although the slope increases slightly with higher PNTA values. The corresponding annualized hazard curve (1 year exposure time) for a single site is shown in Figure 16 along with the annualized probability of 1 m or greater runup from far-field sources determined by empirical analysis (Figure 10). As before, we assume an amplification factor of 2 to convert PNTA to runup. Under these assumptions, the risk from far-field tsunamis at this level (1 m and greater) appears to be slightly greater than that from local tsunamis at this particular site assuming the G–R earthquake distribution model.

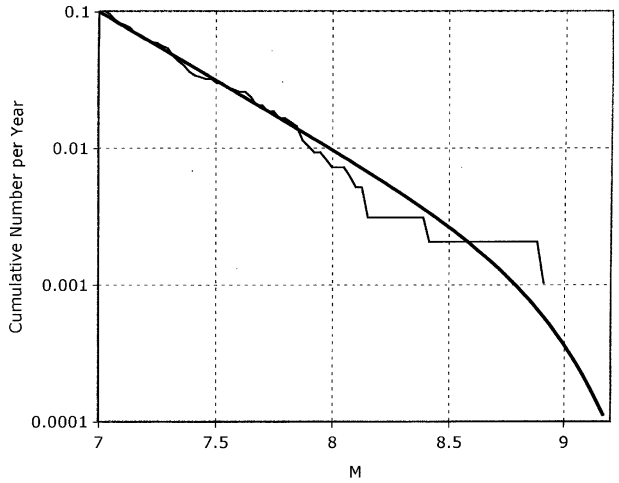

Figure 13. Cumulative number earthquake per year for modified G–R relationship (heavy) and random sample (light) calculated from the distribution shown in Figure 3 and a geologic estimate of the seismic moment budget for the Cascadia seismic zone.

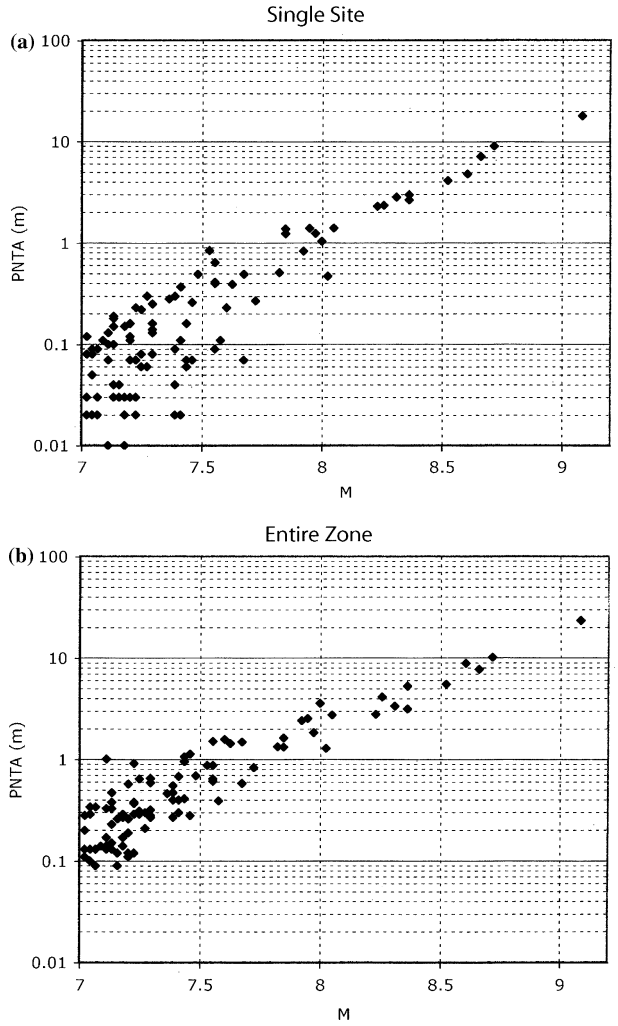

Figure 14. PNTA as a function of earthquake magnitude for a random sample of 100 earthquakes that follow a modified G–R distribution (Figure 13): (a) for a single coastal site at 43.5° N; (b) maximum PNTA in entire seismic zone for each earthquake.

Comparing the local PTHA results from the two regions examined in this study, southern Mexico and Cascadia, differences in the cumulative frequency–runup curves (Figures 8 and 15, respectively) are traced to differences in the seismotectonics of the two regions. The curve for Cascadia is approximately linear (i.e., simple power law relationship), indicating that large events (up to $M \sim 9$ earthquakes) are possible, albeit at low recurrence rates. The potential rupture area for southern Mexico is smaller in width than that for Cascadia, owing to the fact that the lithosphere of the overriding plate in Mexico is thin and composed of oceanic material

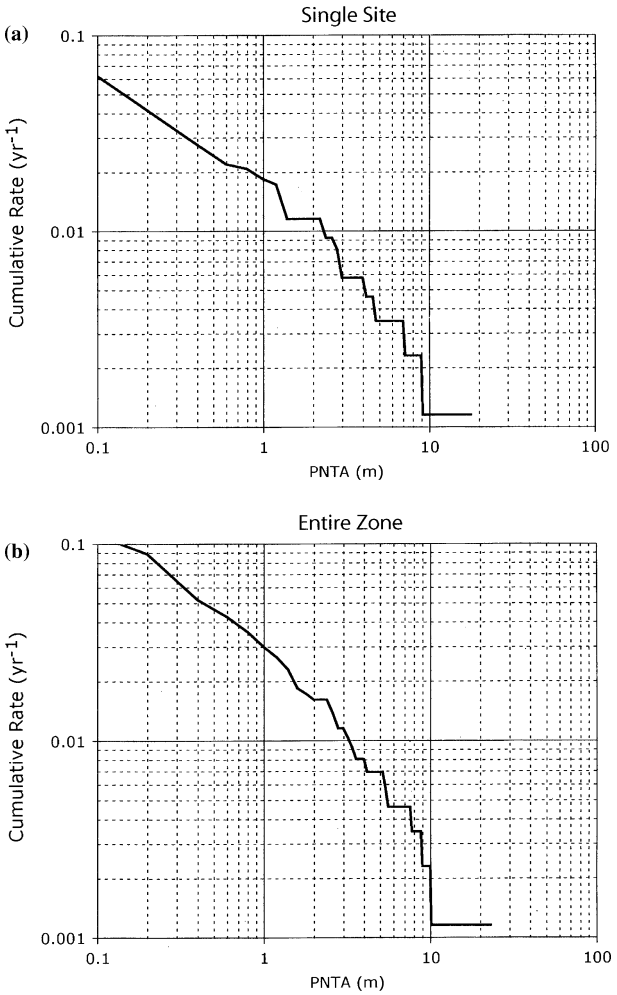

Figure 15. Cumulative frequency–PNTA curves using the modified G–R distribution for (a) a single coastal site (latitude 43.5° N); (b) the entire seismic zone.

(Suárez *et al*., 1990; Suárez and Sánchez, 1996). In this case the frequency–runup curve has a more arcuate tail (Figure 8) indicative of an upper-truncated power-law relationship limited by the maximum earthquake size. From this, we can conclude that it is important to account for regional geologic differences in source parameterization when conducting probabilistic tsunami assessments.

6. Conclusions

In this study, we have shown how methods commonly used in PSHA can be modified for use in PTHA of local tsunamis. The primary difference

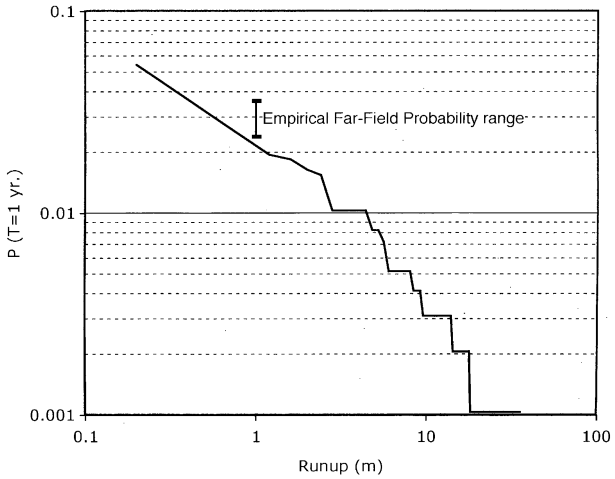

Figure 16. Annualized hazard curve for the site in Figure 15a. Probability calculations assume that earthquakes follow a Poisson process. Because of the low exeedance rates, annualized Poisson probabilities are approximately equal to the exceedance rate curve (Figure 15a). Far-field annualized probability shown for runup >1 m (Figure 10).

between PSHA and PTHA is the need to include far-field sources in tsunami analysis and computational methods to calculate nearshore tsunami amplitudes or runup. As in PSHA, model and parameter uncertainty can be incorporated into PTHA calculations through the use of logic trees or, for the case of inherent variability of slip distribution patterns, through direct integration in the rate calculations. For the latter, a previously developed stochastic source model is used to determine the expected value and deviation of nearshore tsunami amplitudes (Geist, 2002). We also adapt a zonation-based Monte Carlo simulation technique (Ward, 1994) for tsunami analysis in which earthquake magnitudes are defined by a modified G–R distribution and earthquake location and slip distribution are randomized. With accurate source parameterization, these computational techniques can produce synthetic cumulative frequency–runup curves to assess regional or site-specific tsunami hazards. Simpler techniques can be developed for far-field tsunami sources, though in many cases there are sufficient data to perform empirical analyses.

Empirical analysis of tsunami data can serve either as a primary tool to establish site-specific hazard curves or provide regional background information on far-field tsunamis. Results from the Acapulco case study in which empirical analysis was compared to a Monte Carlo simulation of local tsunamis indicate that catalog completeness is an critical factor for determining accurate recurrence rates. In practice, as with earthquake studies (written communication, Art Frankel), different periods of a tsunami

catalog which is complete for a given runup threshold can be used to establish recurrence rates for that runup threshold. A typical tsunami catalog can be divided between observations prior to and following the installation of tide-gauge stations. Sufficient historical observations that pre-date tide-gage measurements can constrain the tail (i.e., high runup) of the cumulative frequency–runup curves (Figure 6), whereas tide-gauge measurements can constrain the low-runup part of this curve where the historical observations are incomplete (Figure 8). In general, empirical analysis is best suited for site-specific studies for which there are sufficient data on tsunami runup. Taken together, results for different completeness periods can yield accurate recurrence estimates for a wide range of tsunami runups. Region-wide hazard assessment where there is a sparse record of tsunamis, as with the Cascadia case-study, is best approached using computational methods, using empirical analysis to provide background information.

Acknowledgements

Maps were prepared using the GMT software (Wessel and Smith, 1995). This paper benefited from comments by Art Frankel and Ned Field as well as by two anonymous reviewers.

References

Abe, K.: 1995. Estimate of tsunami run-up heights from earthquake magnitudes, *Tsunami: Progress in Prediction, Disaster Prevention and Warning*. In Y. Tsuchiya & N. Shuto (Eds.), 21–35: Kluwer Academic Publishers.

Abercrombie, R. E.: 1995, Earthquake source scaling relationships from −1 to 5 ML, using seismograms recorded at 2.5 km depth, *J. Geophys. Res.* **100**, 24015–24036.

Adams, J.: 1990, Paleoseismicity of the Cascadia subduction zone: evidence from turbidites off the Oregon-Washington margin, *Tectonics* **9**, 569–583.

Anderson, J. G. and Brune, J. N.: 1999, Probabilistic seismic hazard analysis without the ergodic assumption, *Seismol. Res. Lett.* **70**, 19–28.

Anderson, J. G., Brune, J. N., Anooshehpoor, R., and Ni, S. D.: 2000, New ground motion data and concepts in seismic hazard analysis, *Curr. Sci.* **79**, 1278–1290.

Atwater, B. F. and Hemphill-Haley, E.: 1997, Recurrence intervals for great earthquakes of the past 3,500 years at northeastern Willapa Bay, Washington. Professional Paper 1576, U.S. Geological Survey, 108 pp.

Baptista, A. M., Priest, G. R., and Murty, T. S.: 1993, Field survey of the 1992 Nicaragua tsunami, *Mar. Geodesy* **16**, 169–203.

Ben-Menahem, A. and Rosenman, M.: 1972, Amplitude patterns of tsunami waves from submarine earthquakes, *J. Geophys. Res.* **77**, 3097–3128.

Bilek, S. L. and Lay, T.: 1999, Rigidity variations with depth along interplate megathrust faults in subduction zones, *Nature* **400**, 443–446.

Bilek, S. L. and Lay, T.: 2000, Depth dependent rupture properties in circum-Pacific subduction zones, In: J. B. Rundle, D. L. Turcotte and W. Klein (eds), *GeoComplexity and the Physics of Earthquakes*, American Geophysical Union, pp. 165–186.

Birkeland, K. W. and Landry, C. C.: 2002, Power-laws and snow avalanches, *Geophys. Res. Lett.* **29**, 49-1–49-3.

Bogen, K.: 1994, A note on compounded conservatism, *Risk Anal.* **14**, 379–381.

Boore, D. M., Joyner, W. B., and Fumal, T. E.: 1997, Equations for estimating horizontal response spectra and peak acceleration from western North American earthquakes: a summary of recent work, *Seismol. Res. Lett.* **68**, 128–153.

Borrero, J. C.: 2001, Changing field data gives better model results: an example from Papua New Guinea. *International Tsunami Symposium 2001*, Seattle, Washington, pp. 397–405.

Borrero, J. C., Ortiz, M., Titov, V. V., and Synolakis, C. E.: 1997, Field survey of Mexican tsunami produces new data, unusual photos, *Eos Trans. Am. Geophys. Union* **78**, 85–88.

Burroughs, S. M. and Tebbens, S. F.: 2001, Upper-truncated power laws in natural systems, *Pure Appl. Geophys.* **158**, 741–757.

Burroughs, S. M. and Tebbens, S. F.: 2005, Power law scaling and probabilistic forecasting of tsunami runup heights, *Pure Appl. Geophys.* **162**, 331–342.

Comer, R. P.: 1980, Tsunami height and earthquake magnitude: theoretical basis of an empirical relation, *Geophys. Res. Lett.* **7**, 445–448.

Coppersmith, K. J. and Youngs, R. R.: 1986, Capturing uncertainty in probabilistic seismic hazard assessments within intraplate tectonic environments, *Proceedings of the Third U.S. National Conference on Earthquake Engineering*, Charleston, South Carolina, pp. 301–312.

Cornell, C. A.: 1968, Engineering seismic risk analysis, *Bull. Seismol. Soc. Am.* **58**, 1583–1606.

Cramer, C. H., Petersen, M. D., and Reichle, M. S.: 1996, A Monte Carlo approach in estimating uncertainty for a seismic hazard assessment of Los Angeles, Ventura, and Orange counties, California, *Bull. Seismol. Soc. Am.* **86**, 1681–1691.

Crawford, P. L.: 1987, Tsunami predictions for the coast of Alaska: Kodiak Island to Ketchikan. Technical Report CERC-87-7, U.S. Army Engineer Waterways Experiment Station, Vicksburg, MS, 137 pp.

DeShon, H. R., Schwartz, S. Y., Bilek, S. L., Dorman, L. M., Gonzalez, V., Protti, J. M., Flueh, E., and Dixon, T. H.: 2003, Seismogenic zone structure of the southern Middle America Trench, Costa Rica, *J. Geophys. Res.* **108**, 12–14 ESE 12–1-ESE.

Downes, G. L. and Stirling, M. W.: 2001, Groundwork for development of a probabilistic tsunami hazard model for New Zealand, *International Tsunami Symposium 2001*, Seattle, Washington, pp. 293–301.

Dziewonski, A. M. and Anderson, D. L.: 1981, Preliminary reference Earth model, *Phys. Earth Planet. Interiors* **25**, 297–356.

Ebel, J. E. and Kafka, A. L.: 1999, A Monte Carlo approach to seismic hazard analysis, *Bull. Seismol. Soc. Am.* **89**, 854–866.

Field, E. H., Jackson, D. D., and Dolan, J. F.: 1999, A mutually consistent seismic-hazard source model for southern California, *Bull. Seismol. Soc. Am.* **89**, 559–578.

Frankel, A. D., Mueller, C. S., Barnhard, T., Perkins, D. M., Leyendecker, E. V., Dickman, N., Hanson S., and Hopper, M.: 1996, National seismic-hazard maps: Documentation June 1996. Open-File Report 96-532, U.S. Geological Survey, 41 pp.

Frankel, A. D., Petersen, M. D., Mueller, C. S., Haller, K. M., Wheeler, R. L., Leyendecke, E. V., Wesson, R. L., Harmsen, S. C., Cramer, C. H., Perkins, D. M., and Rukstales, K. S.: 2002, Documentation for the 2002 Update of the National Seismic Hazard Maps. Open-File Report 02-420, U.S. Geological Survey, 33 pp.

Garcia, A. W. and Houston, J. R.: 1975, Type 16 Flood Insurance Study: Tsunami Predictions for Monterey and San Francisco Bays and Puget Sound. Technical Report H-75-17, U.S. Army Engineer Waterways Experiment Station, Vicksburg, MS, 263 pp.

Geist, E. L.: 1999, Local tsunamis and earthquake source parameters, *Adv. Geophys.* **39**, 117–209.

Geist, E. L.: 2002, Complex earthquake rupture and local tsunamis, *J. Geophys. Res.* **107**, ESE 2-1–ESE 2-16.

Geist, E. L., 2005: Local Tsunami Hazards in the Pacific Northwest from Cascadia Subduction Zone Earthquakes. U.S. Geological Survey Professional Paper 1661-B, 17 pp.

Geist, E. L. and Dmowska, R.: 1999, Local tsunamis and distributed slip at the source, *Pure Appl. Geophys.* **154**, 485–512.

Geist, E. L. and Bilek, S. L.: 2001, Effect of depth-dependent shear modulus on tsunami generation along subduction zones, *Geophys. Res. Lett.* **28**, 1315–1318.

Geller, R. J.: 1976, Scaling relations for earthquake source parameters and magnitudesa, *Bull. Seismol. Soc. Am.* **66**, 1501–1523.

Goldfinger, C., Nelson, C. H., and Johnson, J. E., The Shipboard Scientific Party: 2003, Holocene earthquake records from the Cascadia subduction zone and northern San Andreas fault based on precise dating of offshore turbidites, *Annu. Rev. Earth Planet. Sci.* **31**, 555–577.

González, F. I., Satake, K., Boss, E. F., and Mofjeld, H. O.: 1995, Edge wave and non-trapped modes of the 25 April 1992 Cape Mendocino tsunami, *Pure Appl. Geophys.* **144**, 409–426.

Harmsen, S. C. and Frankel, A. D.: 2001, Geographic deaggregation of seismic hazard in the United States, *Bull. Seismol. Soc. Am.* **91**, 13–26.

Hino, R., Tanioka, Y., Kanazawa, T., Sakai, S., Nishino, M., and Suyehiro, K.: 2001, Micro-tsunami from a local interplate earthquake detected by cabled offshore tsunami observation in northeastern Japan, *Geophys. Res. Lett.* **28**, 3533–3536.

Hirata, K., Takahashi, H., Geist, E. L., Satake, K., Tanioka, Y., Sugioka, H., and Mikada, H.: 2003, Source depth dependence of micro-tsunamis recorded with ocean-bottom pressure gauges; the January 28, 2000 Mw 6.8 earthquake off Nemuro Peninsula, Japan, *Earth Planet. Sci. Lett.* **208**, 305–318.

Horikawa, K. and Shuto, N.: 1983, Tsunami disasters and protection measures in Japan, In: K. Iida and T. Iwasaki (eds), *Tsunamis-Their Science and Engineering*, Terra Scientific Publishing Company, pp. 9–22.

Houston, J. R.: 1980, Type 19 Flood Insurance Study, Tsunami Predictions for Southern California. Technical Report HL-80-18, U.S. Army Engineer Waterways Experiment Station, Vicksburg, MS.

Houston, J. R., Carver, R. D. and Markle, D. G.: 1977, Tsunami-wave elevation frequency of occurrence for the Hawaiian Islands. Technical Report H-77-16, U.S. Army Engineer Waterways Experiment Station, Vicksburg, MS, 66 pp.

Hyndman, R. D. and Wang, K.: 1994, The rupture zone of Cascadia great earthquakes from current deformation and the thermal regime, *J. Geophys. Res.* **100**, 22133–22154.

Iida, K., Cox, D. C., and Pararas-Carayannis, G.: 1967, Preliminary catalog of tsunamis occurring in the Pacific Ocean. HIG 67-10, Hawaii Institute of Geophysics, University of Hawaii, Honolulu, 131 pp.

Imamura, F., Shuto, N., Ide, S., Yoshida, Y., and Abe, K.: 1993, Estimate of the tsunami source of the 1992 Nicaraguan earthquake from tsunami data, *Geophys. Res. Lett.* **20**, 1515–1518.

Ito, K. and Matsuzaki, M.: 1990, Earthquakes and self-organized critical phenomena, *J. Geophys. Res.* **95**, 6853–6860.

Kagan, Y. Y.: 1997, Seismic moment-frequency relation for shallow earthquakes: regional comparison, *J. Geophys. Res.* **102**, 2835–2852.

Kagan, Y. Y.: 1999, Universality of the seismic-moment–frequency relation, *Pure Appl. Geophys.* **155**, 537–573.

Kagan, Y. Y.: 2002a, Seismic moment distribution revisited: II. Moment conservation principle, *Geophys. J. Int.* **149**, 731–754.

Kagan, Y. Y.: 2002b, Seismic moment distribution revisited: I. Statistical Results, *Geophys. J. Int.* **148**, 520–541.

Kagan, Y. Y. and Jackson, D. D.: 1995, New seismic gap hypothesis: five years after, *J. Geophys. Res.* **100**, 3943–3959.

Kagan, Y. Y. and Jackson, D. D.: 2000, Probabilistic forecasting of earthquakes, *Geophys. J. Int.* **143**, 438–453.

Kajiura, K.: 1963, The leading wave of a tsunami, *Bull. Earthquake Res. Inst.* **41**, 535–571.

Kajiura, K.: 1981, Tsunami energy in relation to parameters of the earthquake fault model, *Bull. Earthquake Res. Inst.* **56**, 415–440.

Kanamori, H. and Anderson, D. L.: 1975, Theoretical basis of some empirical relations in seismology, *Bull. Seismol. Soc. Am.* **65**, 1073–1095.

Kockelman, W. J.: 1989, Reducing earthquake hazards in Oregon and Washington: an introduction to the five components necessary for effective hazard reduction. Open-File Report 89-465, U. S. Geological Survey, 190–212 pp.

Lin, I. and Tung, C. C.: 1982, A preliminary investigation of tsunami hazard, *Bull. Seismol. Soc. Am.* **72**, 2323–2337.

Malamud, B. D., Turcotte, D. L., and Barton, C. C.: 1996, The 1993 Mississippi River Flood: a one hundred or a one thousand year event?, *Environ. Eng. Geosci.* **2**, 479–486.

Malamud, B. D., Turcotte, D. L., Guzzetti, F., and Reichenbach, P.: 2004, Landslide inventories and their statistical properties, *Earth Surface Proc. Landforms* **29**, 687–7111.

Matsuyama, M., Walsh, J. P., and Yeh, H.: 1999, The effect of bathymetry on tsunami characteristics at Sissano Lagoon, Papua New Guinea, *Geophys. Res. Lett.* **26**, 3513–3516.

Miller, S. A.: 2002, Earthquake scaling and the strength of seismogenic faults, *Geophys. Res. Lett.* **29**, 27–1–27–4.

Mofjeld, H. O., Foreman, M. G. G., and Ruffman, A.: 1997, West Coast tides during Cascadia subduction zone tsunamis, *Geophys. Res. Lett.* **24**, 2215–2218.

National Research Council (NRC): 1988, *Probabilistic Seismic Hazard Analysis*, National Academy Press, Washington, DC, 97 pp.

National Research Council (NRC): 1997, *Review of Recommendations for Probabilistic Seismic Hazard Analysis: Guidance on Uncertainty and Use of Experts*, National Academy Press, Washington, DC, 73 pp.

Ortiz, M., Kostoglodov, V., Singh, S. K., and Pacheco, J. F.: 2000, New constraints on the uplift of October 9, 1995 Jalisco-Colima earthquake (Mw 8) based on the analysis of tsunami records at Manzanillo and Navidad, Mexico, *Geofisica Int.* **39**, 349–357.

Pacheco, J. F., Scholz, C. H., and Sykes, L. R.: 1992, Changes in frequency-size relationship from small to large earthquakes, *Nature* **355**, 71–73.

Parsons, T., Trehu, A. M., Luetgert, J. H., Miller, K., Kilbride, F., Wells, R. E., Fisher, M. A., Flueh, E., ten Brink, U. S., and Christensen, N. I.: 1998, A new view into the Cascadia subduction zone and volcanic arc: implications for earthquake hazards along the Washington margin, *Geology* **26**, 199–202.

Pelayo, A. M. and Wiens, D. A.: 1992, Tsunami earthquakes: slow thrust-faulting events in the accretionary wedge, *J. Geophys. Res.* **97**, 15321–15337.

Petersen, M. D., Cramer, C. H., and Frankel, A. D.: 2002, Simulations of seismic hazard for the Pacific Northwest of the United States from earthquakes associated with the Cascadia subduction zone, *Pure Appl. Geophys.* **159**, 2147–2168.

Pisarenko, V. F. and Sornette, D.: 2004, Statistical detection and characterization of a deviation from the Gutenberg–Richter distribution above magnitude 8, *Pure Appl. Geophys.* **161**, 839–864.

Polet, J. and Kanamori, H.: 2000, Shallow subduction zone earthquakes and their tsunamigenic potential, *Geophys. J. Int.* **142**, 684–702.

Rabinovich, A. B.: 1997, Spectral analysis of tsunami waves: separation of source and topography effects, *J. Geophys. Res.* **102**, 12663–12676.

Rikitake, T. and Aida, I.: 1988, Tsunami hazard probability in Japan, *Bull. Seismol. Soc. Am.* **78**, 1268–1278.

Romanowicz, B. and Rundle, J. B.: 1993, On scaling relationships for large earthquakes, *Bull. Seismol. Soc. America* **83**, 1294–1297.

Rong, Y., Jackson, D. D. and Kagan, Y. Y.: 2003, Seismic gaps and earthquakes, *J. Geophys. Res.* **108**, ESE 6–1 −6–14.

Rubinstein, R. Y.: 1981, *Simulation and the Monte Carlo Method*, Wiley, 278 pp.

Rundle, J. B.: 1989, Derivation of the complete Gutenberg–Richter magnitude-frequency relation using the principle of scale invariance, *J. Geophys. Res.* **94**, 12337–12342.

Sanchez, A. J. and Farreras, S. F.: 1993, Catalog of tsunamis on the western coast of Mexico. World Data Center A for Solid Earth Geophysics Publication SE-50, National Geophysical Data Center, Boulder, Colorado, 79 pp.

Satake, K.: 2002, Tsunamis. In: W. H. K. Lee, H. Kanamori, P. C. Jennings and C. Kisslinger (eds), *International Handbook of Earthquake and Engineering Seismology*, International Association of Seismology and Physics of the Earth's Interior, pp. 437–451.

Satake, K., Wang, K., and Atwater, B.F.: 2003, Fault slip and seismic moment of the 1700 Cascadia earthquake inferred from Japanese tsunami descriptions, *J. Geophys. Res.* **108**, ESE 7-1–7-17.

Savage, J. C.: 1991, Criticism of some forecasts of the National Earthquake Prediction Evaluation Council, *Bull. Seismol. Soc. Am.* **81**, 862–881.

Savage, J. C.: 1992, The uncertainty in earthquake conditional probabilities, *Geophys. Res. Lett.* **19**, 709–712.

Scholz, C. H.: 1982, Scaling laws for large earthquakes: consequences for physical models, *Bull. Seismol. Soc. Am.* **72**, 1–14.

Schwartz, S. Y.: 1999, Noncharacteristic behavior and complex recurrence of large subduction zone earthquakes. *J. Geophys. Res.* **104**, 23111–23125.

Senior Seismic Hazard Analysis Committee (SSHAC): 1997, Recommendations for Probabilistic Seismic Hazard Analysis: Guidance on Uncertainty and Use of Experts. Main Report NUREG/CR-6372 UCRL-ID-122160 Vol. 1, U.S. Nuclear Regulatory Commission, 256 pp.

Shaw, B. E. and Scholz, C. H.: 2001, Slip-length scaling in large earthquakes: observations and theory and implications for earthquake physics, *Geophys. Res. Lett.* **28**, 2995–2998.

Shuto, N.: 1991, Numerical simulation of tsunamis – its present and near future, *Nat. Hazards* **4**, 171–191.

Singh, S. K., Rodriguez, M., and Esteva, L.: 1983, Statistics of small earthquake and frequency of occurrence of large earthquakes along the Mexican subduction zone, *Bull. Seismol. Soc. Am.* **73**, 1779–1796.

Soloviev, S. L.: 1969, Recurrence of tsunamis in the Pacific. In: W. M. Adams (ed.), *Tsunamis in the Pacific Ocean*, East-West Center Press, pp. 149–163.

Soloviev, S. L. and Go, Ch. N.: 1984: Catalog of tsunamis on the eastern shore of the Pacific Ocean. Canadian Translation of Fisheries and Aquatic Sciences No. 5078, Canada Insitute for Scientific and Technical Information, Ontario, Canada, 285 pp.

Somerville, P., Irikura, K., Graves, R., Sawada, S., Wald, D., Abrahamson, N. A., Iwasaki, Y., Kagawa, T., Smith, N., and Kowada, A.: 1999, Characterizing crustal earthquake slip models for the prediction of strong ground motion, *Seismol. Res. Lett.* **70**, 59–80.

Sornette, D. and Virieux, J.: 1992, Linking short-timescale deformation to long-timescale tectonics, *Nature* **357**, 401–404.

Suárez, G. and Sánchez, O.: 1996, Shallow depth of seismogenic coupling in southern Mexico: implications for the maximum size of earthquakes in the subduction zone, *Phys. Earth Planet. Int.* **93**, 53–61.

Suárez, G., Monfret, T., Wittlinger, G., and David, C.: 1990, Geometry of subduction and depth of the seismogenic zone in the Guerrero gap, Mexico, *Nature* **345**, 336–338.

Tadepalli, S. and Synolakis, C. E.: 1996, Model for the leading waves of tsunamis, *Phys. Rev. Lett.* **77**, 2141–2144.

Tanioka, Y. and Satake, K.: 1996, Tsunami generation by horizontal displacement of ocean bottom, *Geophys. Res. Lett.* **23**, 861–865.

Tichelaar, B. W. and Ruff, L. J.: 1993, Depth of seismic coupling along subduction zones, *J. Geophys. Res.* **98**, 2017–2037.

Tinti, S. and Armigliato, A.: 2003, The use of scnarios to evaluate the tsunami impact in southern Italy, *Mar. Geology* **199**, 221–243.

Titov, V. V. and Synolakis, C. E.: 1997, Extreme inundation flows during the Hokkaido-Nansei-Oki tsunami, *Geophys. Res. Lett.* **24**, 1315–1318.

Toro, G. R., Abrahamson, N. A., and Schneider, J. F.: 1997, Model of strong ground motions from earthquakes in central and eastern North America: best estimates and uncertainties, *Seismol. Res. Lett.* **68**, 41–57.

U.S. Interagency Advisory Committee on Water Data: 1982, Guidelines for determining flood flow frequency. Bulletin 17-B of the Hydrology Subcommittee, U.S. Geological Survey, Office of Water Data Coordination, Reston, Virginia, 183 pp.

Valdes, C. M., Mooney, W. D., Singh, S. K., Meyer, R. P., Lomnitz, C., Luetgert, J. H., Helsley, C. E., Lewis, B. T. R., and Mena, M.: 1986, Crustal structure of Oaxaca, Mexico, from seismic refraction measurements, *Bull. Seismol. Soc. Am.* **76**, 547–563.

Vere-Jones, D., Robinson, R., and Yang, W.: 2001, Remarks on the accelerated moment release model: problems of model formulation, simulation and estimation, *Geophys. J. Int.* **144**, 517–531.

Ward, S. N.: 1980, Relationships of tsunami generation and an earthquake source, *J. Phys. Earth* **28**, 441–474.

Ward, S. N.: 1982, On tsunami nucleation II. An instantaneous modulated line source, *Phys. Earth Planet. Int.* **27**, 273–285.

Ward, S. N.: 1991, A synthetic seismicity model for the Middle America trench, *J. Geophys. Res.* **96**, 21433–21442.

Ward, S. N.: 1992, An application of synthetic seismicity in earthquake statistics: The Middle America trench, *J. Geophys. Res.* **97**, 6675–6682.

Ward, S. N.: 1994, A multidisciplinary approach to seismic hazard in southern California, *Bull. Seismol. Soc. Am.* **84**, 1293–1309.

Ward, S. N.: 1996, A synthetic seismicity model for southern California: cycles, probabilities and hazards, *J. Geophys. Res.* **101**, 22393–22418.

Ward, S. N.: 2000, San Francisco Bay area earthquake simulations: a step toward a standard physical earthquake model, *Bull. Seismol. Soc. Am.* **90**, 370–386.

Ward, S. N.: 2001, Landslide tsunami, *J. Geophys. Res.* **106**, 11201–11215.

Ward, S. N.: 2002, Tsunamis, In: R. A. Meyers (ed.), *The Encyclopedia of Physical Science and Technology*, Academic Press, pp. 175–191.

Ward, S. N. and Asphaug, E.: 2000, Asteroid impact tsunami: a probabilistic hazard assessment, *Icarus* **145**, 64–78.

Wells, D. L. and Coppersmith, K. J.: 1994, New empirical relationships among magnitude, rupture length, rupture width, rupture area, and surface displacement, *Bull. Seismol. Soc. Am.* **84**, 974–1002.

Wesnousky, S. G.: 1994, The Gutenberg–Richter or characteristic earthquake distribution, which is it?, *Bull. Seismol. Soc. Am.* **84**, 1940–1959.

Wessel, P. and Smith, W. H. F.: 1995, New version of the Generic Mapping Tools released, *Eos Trans. Am. Geophys. Union* **76**, F329.

Wyss, M.: 1979, Estimating maximum expectable magnitude of earthquake from fault dimensions, *Geology* **6**, 336–340.

Youngs, R. R., Arabasz, W. J., Anderson, R. E., Ramelli, A. R., Ake, J. P., Slemmons, D. B., McCalpin, J. P., Doser, D. I., Fridrich, C. J., Swan, F. H. III, Rogers, A., Yount, J. C., Anderson, L. W., Smith, K. D., Bruhn, R. L., Knuepfer, P. L. K., Smith, R. B., dePolo, C. M., O'Leary, D. W., Coppersmith, K. J., Pezzopane, S. K., Schwartz, D. P., Whitney, J. W., Olig, S. S., and Toro, G. R.: 2003, A methodology for probabilistic fault displacement hazard analysis (PFDHA), *Earthquake Spectra* **19**, 191–219.